AN ABSTRACT OF THE THESIS OF

THOMAS BRIAN CURTIN for the MASTER OF SCIENCE
(Degree)

in OCEANOGRAPHY presented on August 14, 1970
(Major) (Date)

Title: TOWED ELECTRODES IN THE SEA: THEORY AND USE

Redacted for privacy

Abstract approved: _____
Stephen J. Neshyba

The sea as a dynamic conducting medium interacts continually with the earth's magnetic field. The physical principles underlying this interaction are reviewed. These results are applied to the particular problem of towed electrodes at the sea surface. Data using this method are then shown to be sensitive to stability oscillations especially in lower latitudes. Finally, some features of the water velocity around the Panama Basin are investigated from towed electrode measurements.

Towed Electrodes in the Sea: Theory and Use

by

Thomas Brian Curtin

A THESIS

submitted to

Oregon State University

in partial fulfillment of
the requirements for the
degree of

Master of Science

June 1970

APPROVED:

Redacted for privacy

Associate Professor of Oceanography
in charge of major

Redacted for privacy

Chairman of Department of Oceanography

Redacted for privacy

Dean of Graduate School

Date thesis is presented August 14, 1970

Typed by Sammy McMurphey for Thomas Brian Curtin

TABLE OF CONTENTS

		Page
I.	Introduction	1
	A. Review	1
	B. Objectives	2
II.	Steady-State Field	4
	A. General Principles (Basic Theory of the Electrical Field in the Sea)	4
	B. The Geomagnetic Electrokinetograph	7
	1. Description	7
	2. Theory of Operation	8
	C. The Signal Measured Over Two Specified Velocity Models	12
	D. A Suggested Technique for Interpretation of GEK Records	31
III.	Time-Dependent Effects	35
	A. General	35
	B. Electromagnetic Effects	36
	C. Hydromagnetic Effects	40
IV.	Observations of Stability Oscillations	44
	A. Observational Data	44
	B. Specific Analysis	49
	C. Conclusions	57
V.	Velocity Observations Around the Panama Basin	60
	A. General	60
	B. Method of Analysis	61
VI.	Summary and Conclusions	72
Bibliography		74
Appendices		
	Appendix A (A note on electromagnetic units)	77
	Appendix B	
	Silver-silver chloride electrodes	81
	State-of-the-art	81
	Some further experiments	85
	Electrode Design	85
	Electrode flow reaction	88

LIST OF FIGURES

Figure		Page
1	Solutions for a rectangular current that is wide compared to the depth.	17
2	Solutions for a rectangular current that is narrow compared to the depth.	23
3	Solutions for a periodic current that is wide compared to the depth.	29
4	Solutions for a periodic current that is narrow compared to the depth.	30
5	Electromagnetic characteristics as functions of parameters of oceanic scale.	39
6	Dimensionless hydromagnetic numbers as functions of parameters of oceanic scale.	41
7	Lines along which oscillations of two minute order were observed in the measured signal.	45
8	Examples of the type of signal measured by towed electrodes at positions indicated in Figure 7.	46
9	Temperature (A) and salinity (B) sections from the Galapagos Islands to the Ecuadorian coast as shown in Figure 7-C.	50
10	The Brunt-Väisälä frequency as a function of depth for positions indicated in Figure 7.	52
11	The Brunt-Väisälä frequency as a function of depth for positions indicated in Figure 7.	58
12	Maximum current vectors measured by GEK along the perimeter of the Panama Basin in the eastern tropical Pacific Ocean.	62

13 The signal from towed electrodes measured between the Galapagos Islands and the Costa Rica coast. The stippled curve indicates the smoothed average. 64

14 The signal from towed electrodes measured between Ecuador and the Galapagos Islands. The stippled curve indicates the smoothed average. 65

15 Current pattern for the East Tropical Pacific Ocean. (a) Pattern as previously compiled by Wyrtki (1965). (b) Contrasting strong surface currents recorded by GEK. (Note direction from N and NE) 68

LIST OF FIGURES IN APPENDICES

B-1 Potential of sea water concentration cell versus time for S_1 = 37‰ and S_2 = 29.6‰. (After Sanford, 1967) 84

B-2 The potential difference between two well-soaked electrodes (silver-silver chloride) immersed in sea water under completely static conditions was recorded for 48 hours. These are representative portions of the resulting record. Densely inked areas correspond to high frequency pen movement. (See text for details.) 87

B-3 Hypothetical detailed structure of the electrolyte double layer (Barlow and MacDonald, 1967). 90

B-4 Electrical potential developed by direct wave-induced flow past silver-silver chloride electrodes in a long narrow tank. Arrows (⟶) indicate direction of water velocity. 91

B-5 Electrical potential developed by a complicated flow past silver-silver chloride electrodes in a larger (see text) tank. 95

LIST OF TABLES

Table		Page
1	Fundamental relations	5
2	Velocity distributions previously considered	13
3	Solutions for distributions D and E	15
4	Definitions of terms	37
5	Average oceanic values	38
A. 1	Rationalized MKS system-Gaussian system	79

LIST OF SYMBOLS

A - Alfvén number

$\vec{A}$ - the magnetic vector potential

$\vec{B}$ - the magnetic induction field

b - the width of unidirectional velocity

c - the speed of light

$\vec{D}$ - the electric displacement field

d - the depth of the thermocline

d_η - the electromagnetic penetration depth

d_h - Hartmann depth

$\vec{E}$ - the total electric field

f - the coriolis force

g - the conductivity of seawater

$\vec{H}$ - the magnetic intensity field

h - the depth of the water

h' - the depth of the current

$\vec{i}$ - the electric current density

$\vec{k}$ - the wave number

L - the characteristic length scale

Lu - Lundquist number

M - Hartmann number

$\vec{M}$ - the magnetic magnetization field

N - Brunt-Väisälä frequency

$\vec{P}$ - the electric polarization field

p - pressure

p_m - the magnetic Prandtl number

q - the electric charge

R_m - the magnetic Reynolds number

r - the radius of curvature

T - the characteristic time scale

t - time

U - the characteristic velocity

$\vec{V}$ - the velocity vector

V' - Alfvén velocity

x - positive eastward

y - positive northward

z - positive upward (0 at sea surface)

α - radian width of unidirectional velocity

Γ - the ratio of horizontal to vertical magnetic field components

δ' - volume electric charge density

ϵ_o - permittivity of free space

η - magnetic diffusivity

μ_o - permeability of free space

ν - kinematic viscosity

ρ - resistivity of seawater

ρ' - mass density

σ - frequency

σ' - surface electric charge density

τ_{η} - electromagnetic diffusion time

τ_{hm} - hydromagnetic response time

ϕ - electric scalar potential

TOWED ELECTRODES IN THE SEA: THEORY AND USE

I. INTRODUCTION

A. Review

Since the ocean is an electrically conducting geophysical fluid within a quasi-static magnetic field, some information about its velocity structure can be obtained by monitoring the electrical or magnetic variables produced by its motion. First attempts with this method date back to the early nineteenth century (Faraday, 1832). Historical reviews of previous investigations are given by Longuet-Higgins and Barber (1946), von Arx (1950), and Sanford (1967).

The general analytical form of the relationship between the electrical and velocity fields in the ocean was first given by Stommel (1948); empirical results and comparisons were comprehensively presented by von Arx (1950). The latter author incorrectly stated the governing field equations, and valid theoretical foundations of the method were derived in two subsequent papers. Malkus and Stern (1952) demonstrated through an integration technique the relationship between the potential gradient and the total fluid transport. Longuet-Higgins, Stern and Stommel (1954) presented a generic theoretical treatment setting forth the basic governing equations with solutions for several defined velocity fields. Knauss and Reid (1957) correctly estimated some errors introduced by experimental technique despite some invalid analytical statements. Hughes (1962) has presented an

excellent treatment of towed electrodes in shallow water. Most recently, Sanford (1967) has generalized the analysis by considering the electric and velocity fields from a three-dimensional view.

B. Objectives

In general, motional electric fields in the sea can be detected either by stationary or towed electrodes, the latter method being the subject of this investigation. The original proposition underlying the towed method was that the measurement of the horizontal electrical potential gradient in the sea by a moving electrode system could be interpreted as a meaningful indication of the velocity structure. The purpose of this dissertation is not to propose and prove a new thesis, but to review, extend, and demonstrate this proposal.

The usual technique of measuring the horizontal electrical potential gradient is that of towing two electrodes a few shiplengths behind a vessel underway. The electrodes are normally separated by a distance of 100 meters, with each electrode attached to the end of a long conducting wire. This instrument has been called the "geomagnetic electrokinetograph" (GEK) and is described in detail by von Arx (1950). In order to promote understanding and reliability in the use of this technique, the underlying principles and pertinent analytical statements are reviewed and summarized. Some suggestions in interpretive outlook are offered. The effects of time-dependent motion are estimated by considering the sea from a mag-

netohydrodynamical viewpoint. Finally two interesting field observations are presented and analyzed: the manifestation of internal waves in some GEK records, and the electrical and velocity fields measured around the Panama Basin.

II. STEADY-STATE FIELD

A. General Principles
(Basic Theory of the Electrical Field in the Sea)

The ocean when considered as a moving conductor can be described by the classical relationships of electromagnetic theory. As a fluid it also adheres to the principles of hydrodynamics. For reference, some pertinent expressions are listed in Table 1. The units of measurement have been somewhat confusing in electromagnetics and these are examined in Appendix A.

Equation II. 7 and the divergence of this equation can be written, respectively,

$$\vec{i} = g(-\nabla \phi + \vec{V} \times \vec{B}) \qquad \text{II. 15}$$

$$\nabla^2 \phi = \vec{B} \cdot \nabla \times \vec{V} \qquad \text{II. 16}$$

if the following assumptions are taken,

1) the electric field can be represented as the gradient of a scalar potential ($\frac{\partial \vec{A}}{\partial t} = 0$ in equation II. 9);
2) $\vec{B}$ is constant in space ($\nabla \times \vec{B} = 0$);
3) the charge density, δ', is time independent; and
4) the conductivity gradient is zero.

The conditions in the ocean for which assumptions (1) and (2) are true is the subject of chapter III.

In the absence of magnetic material (M = 0) equation II. 13 shows

Table 1. Fundamental Relations

Historical Name*	Relation (MKS-rationalized)	
Gauss' Law	$\nabla \cdot \vec{E} = \rho'/\epsilon_o$	II.1
Coulomb's Law	$\vec{E} = \frac{1}{4\pi\epsilon_o}\int \frac{\delta \vec{r}}{\lvert\vec{r}\rvert^3}\, dv$	II.2
Ampere's Law	$\nabla \times \vec{B} = \mu_o(\vec{i} + \epsilon_o \frac{\partial \vec{E}}{\partial t})$	II.3
Law of Biot and Savart	$\vec{B} = \frac{\mu_o}{4\pi}\int \frac{(\vec{i} + \epsilon_o \frac{\partial \epsilon}{\partial t}) \times \vec{r}}{\lvert\vec{r}\rvert^3}\, dv$	II.4
Single Magnetic Poles Unobserved	$\nabla \cdot \vec{B} = 0$	II.5
Faraday's Law	$\nabla \times \vec{E} = -\frac{\partial \vec{B}}{\partial t}$	II.6
Ohm's Law	$\vec{i} = g(\vec{E} + \vec{V} \times \vec{B})$ (Lorentz Force = $\vec{F} = g\vec{V}\times\vec{B}$)	II.7
Magnetic Vector Potential ($\vec{A}$)	$\vec{B} = \nabla \times \vec{A}$	II.8
Electric Scalar Potential (ϕ)	$\vec{E} = -\nabla\phi - \frac{\partial \vec{A}}{\partial t}$	II.9
Conservation of Charge	$\nabla \cdot \vec{i} + \frac{\partial \delta'}{\partial t} = 0$	II.10

(Table 1 continued)

Magnetic Continuity	$\nabla \cdot \vec{A} + \frac{1}{C^2} \frac{\partial \phi}{\partial t} = 0$	II.11
Electric Displacement Field	$\vec{D} = \epsilon_o \vec{E} - (-\vec{\rho})$	II.12
Magnetic Intensity Field	$\vec{H} = \frac{1}{\mu_o} \vec{B} - \vec{M}$	II.13
Incompressibility Condition	$\nabla \cdot \vec{V} = 0$	II.14

* not entirely uncontroversial

that the magnetic intensity field may be substituted for the magnetic induction field, if the magnetic permeability is unity. This substitution is common, although it should be noted that in MKS-rationalized units a factor of 10^6 is introduced. This is important for practical calculations. With this change equations II. 16 and II. 15 become, respectively,

$$\nabla^2 \phi = \vec{H} \cdot \nabla \times \vec{V} \qquad \text{II. 17}$$

$$\rho \vec{i} = - \nabla \phi + \vec{V} \times \vec{H} \qquad \text{II. 18}$$

These are the basic field equations relating the electrical and velocity fields in the ocean, in a frame of reference fixed on the earth.

B. The Geomagnetic Electrokinetograph

1. Description

The GEK method of measuring the voltage expressed by equation II. 18 employs a high impedance voltmeter and two electrodes arranged as follows (in plan view),

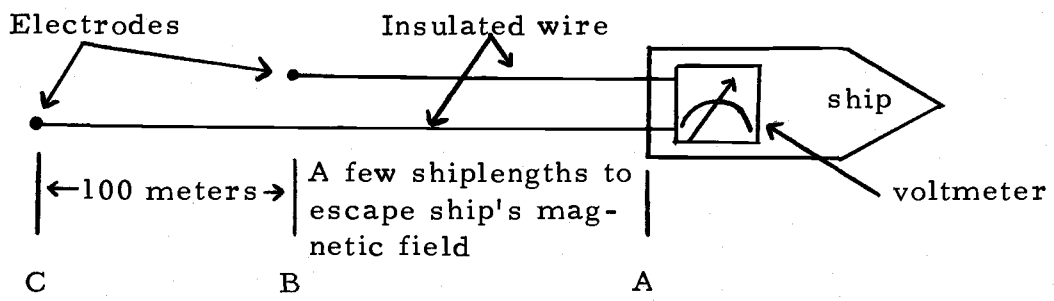

The measuring circuit consists of the voltmeter, the electrode-terminated wires, and the sea-water path between electrodes. The voltmeter is a self-recording potentiometric type of balanced bridge circuit design with extremely high input impedance, thus allowing essentially no electrical current to flow in the measuring circuit.

The electrodes now widely used in GEK measurements are the silver-silver chloride type. They are deployed in pairs which have been "matched" from the standpoint of identical self-potential characteristics when immersed in sea water. When in use as above, the electrodes are specially housed to reduce the undesired potential differences which can arise from temperature and salinity gradients between electrodes, and to eliminate changes in self-potential when an electrode is exposed to direct fluid flow. A more detailed discussion of electrodes is given in Appendix B.

2. Theory of Operation

The potential field per unit distance along any moving conducting path in a magnetic field is always the difference between two electromotive forces (emf's). The first emf per unit distance can be shown by Faraday's law (equation II. 6) to be $(\vec{V} \times \vec{H})$ (Longuet-Higgins, Stern, and Stommel, 1954), where the velocity of the conducting path is $\vec{V}$ and the magnetic field intensity is $\vec{H}$. The second emf per unit distance is $\rho\vec{i}$, as expressed by Ohm's law (equation II. 7) in a sta-

tionary reference frame, where ρ is the resistivity and $\vec{i}$ the current density along the path. Thus, if the potential is represented by ϕ, the electric field in any moving conducting path can be expressed as,

$$\nabla \phi = (\vec{V} \times \vec{H}) - \rho\vec{i}$$

Two separate moving conducting paths are present when considering towed electrodes in the sea: the ocean water itself and the long wires contained in the measuring circuit. The potential in each of these paths is the difference of the two terms $(\vec{V} \times \vec{H})$ and $(\rho\vec{i})$ for each path respectively.

Consider the sea-water path. When electrodes are able to stand directly behind, as indicated in the above diagram, the electrodes measure the potential difference along a path parallel to the direction of ship's heading. The component of emf generated in this direction by the $(\vec{V} \times \vec{H})$ term is $(V_y H_z - V_z H_y)$ where V_y is the water velocity perpendicular to the ship (the set of the ship), V_z is the vertical water velocity, H_z is the vertical intensity of the earth's magnetic field, and H_y is the horizontal geomagnetic field intensity perpendicular to ship heading. If V_z is assumed negligible compared to V_y, this measurable emf per unit distance generated by the water motion is $(V_y H_z)$, that is, the emf contributed by the $(\vec{V} \times \vec{H})$ term is due primarily to the component of water velocity perpendicular to the ship's heading. This water motion is the cause of the ship's set

and is independent of the ship's velocity in the direction parallel to the electrode line. The second emf, $\rho\vec{i}$, in the sea-water path is a direct function of the electrical current density along the path between electrodes. The electrical current density along this path depends on the electrical characteristics (for example, emf's and resistances) of all other surrounding paths, since it is only through the surrounding paths that any closed electrical-current-carrying circuit can be formed.

Now consider the closed conducting path formed by the two electrode-terminated wires, the sea water between electrodes, and the voltmeter, as illustrated above. By identical reasoning to the sea-water path, the velocity induced emf per unit distance in the wires is $(V_y H_z)$. Again this velocity component, V_y, is the set of the ship. The second emf, $\rho\vec{i}$, in this path is essentially zero due to the high impedance of the voltmeter.

GEK data are the voltage differences continuously recorded on the voltmeter. The potential differences the voltmeter "sees" are those developed in the wires to each electrode and in the sea water between the electrodes. Traversing around this path and adding the potentials gives,

$$E_{measured} = (V_y H_z)_{AB} + \left[(V_y H_z)_{BC} - (\rho i_x)_{BC}\right] + (-V_y H_z)_{CB} + (-V_y H_z)_{BA}$$

where A, B, C are the points shown in part 1. The bracketed term represents the potential gradient in the sea water between electrodes; the other terms are the induced emf in the indicated sections of the wire. This experession reduces to:

$$E_{measured} = (\rho i_x)_{BC}$$

where the direction is that of the electrode line. Thus, the quantity that the voltmeter records is:

$$E(volts)_{measured} = \int_B^C \rho i_x dx$$

The electrical current density, $\vec{i}$, in any region is a direct function of the conducting path in which it exists. Thus in the ocean, with the assumption of uniform resistivity, the current density integrated along any line is directly dependent on the emf's in the available return sea-water paths surrounding that line. These emf's, as shown in part A, are directly related to the velocity of the water in the region. Any electrical current density measured at the surface is always a reflection, in part, of the velocity field in the entire water column below.

There is one further source of emf in the measuring circuit. This is the self-potential of the electrodes themselves due to the fact that they are, of necessity, metals emmersed in an electrolyte. Electrode polarization is discussed in Appendix B.

C. The Signal Measured Over Two Specified Velocity Models

As an aid to interpreting the recorded signal on the voltmeter in terms of surrounding oceanic conditions, velocity structures can be assumed and their resulting electrical fields analyzed. Comparison of these known fields with actual data may then possibly indicate a generative source of the signal.

Specifically this process is performed by solving equation II. 17 for a given velocity structure and boundary conditions ($\vec{H}$ being the geomagnetic field), and then using equation II. 18 to find $\rho\vec{i}$. Table 2 lists the velocity fields for which this has been done. ("L-HSS" refers to Longuet-Higgins, Stern and Stommel, 1954.)

Sanford has presented the solution for the most general three-dimensional case, and more specifically for some models of the Gulf Stream. His results can be usefully applied to a particular velocity structure by numerical transform techniques. L-HSS have examined some two-dimensional stream models and solved for their corresponding electrical current densities. Of all the velocity fields thus far considered and listed in Table 2, the two-dimensional rectangular (D) and periodic (E) solutions offer the most utility for general oceanographic field use. Although not providing the precision and accuracy of Sanford's results, they nevertheless provide a sound basis for rapid interpretation of towed electrode measurements without relying on numerical techniques. By illustrating the influence of

Table 2. Velocity Distributions Previously Considered.

				Investigator
A	$\vec{V}(x, y, z, t) = (V_x, V_z, 0)$		$0 \geq z \geq -h$	Sanford (1967)
	$\vec{V}(x, y, z, t) = (0, 0, 0)$		elsewhere	
B	$\vec{V}(x, y, z, t) = (V_o \operatorname{sech} kx(1 + \epsilon e^{i(hy-\omega t)}), 0, 0)$		$0 \geq z \geq -h$	Sanford (1967)
	$\vec{V}(x, y, z, t) = (0, 0, 0)$		elsewhere	
C	$\vec{V}(x, z) = (0, V_o / 1 + (\beta x)^2, 0)$	$-\infty < x < \infty$	$0 \geq z \geq -h'$	Sanford (1967)
	$\vec{V}(x, z) = (0, 0, 0)$		$-h' \geq z \geq -h$	
D	$\vec{V}(x, z) = (0, V, 0)$	$-a < x < a$	$0 \geq z \geq -h'$	Sanford (1967)
	$\vec{V}(x, z) = (0, 0, 0)$	elsewhere	$-h' > z \geq -h$	L-HSS (1954)
E	$\vec{V}(x, z) = (0, V \cos \alpha x, 0)$	$-a < x < a$	$0 \geq z \geq -h'$	L-HSS (1954)
	$\vec{V}(x, z) = (0, 0, 0)$	elsewhere	$-h' > z \geq -h$	
F	$\vec{V}(x, z) = (0, V, 0)$	$-a < x < a$	$0 \geq z \geq -\sqrt{b^2 - \frac{b^2}{a^2} x^2}$	L-HSS (1954)
	$\vec{V}(x, z) = (0, 0, 0)$	elsewhere	$-\sqrt{b^2 - \frac{b^2}{a^2} x^2} > z \geq -h$	L-HSS (1954)

the more important parameters affecting the measurement, this approach lessens the chance of misinterpretation. Finally, the general form of these two fields allows most ocean currents to be modelled to first order by a superposition of solutions.

Table 3 lists the analytical forms of the measured signal recorded by electrodes towed at the surface across the velocity fields defined by D and E of Table 2. These solutions were given by L-HSS. Figures 1 through 4 show graphically the form of these solutions for various parametric values. The rectangular model, defined by D in Table 2 with the solution listed in Table 3, is shown for the two cases of a wide stream (Figure 1), whose width, a, is equal to at least 1.5 times the total water depth; and a narrow stream (Figure 2), whose width, a, is in the order of 1/4 of the total water depth. Similarly for the sinusoidal model (E in Table 2), the case of the wide stream (Figure 3), with width, b, of order 8 times the total depth, and the case of the narrow stream (Figure 4) where b is about 1/2 the water depth are both illustrated. Each of figures 1 through 4 is plotted for different values of the parameter Γ, which is the ratio of the horizontal geomagnetic field component in the direction of the ship's heading to the local vertical geomagnetic field component. Finally for each Γ in each figure there is a complete family of curves corresponding to different values of the ratio of the depth to which the velocity exists to the total water depth (h'/h). Several curves of this family are plotted in each part of each figure.

Table 3. Solutions for Distributions D and E

D: $$(\rho i_x)_{z=0} = VH_z \{ [F(\frac{x+a}{h}) - F(\frac{x+a}{h})] + \Gamma [G(\frac{x+a}{h}) - G(\frac{x-a}{h})]\}$$

$$F(\xi) = \frac{1}{\pi} \tan^{-1} (\tan \frac{h-h'}{h} \frac{\pi}{2} \tanh \frac{\xi\pi}{2})$$

$$G(\xi) = -\frac{1}{2\pi} \log (1 + \frac{\sin^2 \frac{h'}{h} \frac{\pi}{2}}{\sinh^2 \frac{\xi \pi}{2}})$$

Approximations:

i) wide stream ($2a > h$): $$(\rho i_x)_{z=0} = (V_s - \overline{V})H_z + \frac{d\overline{V}}{dx} hH_x - (\rho i_x)_{z=-h}$$

ii) narrow stream ($a \ll h$): $$(\rho i_x)_{z=0} = 2aVH_z \frac{d}{dx} F(\frac{x}{h})$$

E: $$(\rho i_x)_{z=0} = VH_o \cos (\alpha x + \epsilon)$$

$$H_o = (H_z^2 \nu^2 + H_x^2 \nu'^2)^{1/2}$$

$$\tan \epsilon = \Gamma \frac{\nu'}{\nu}$$

$$\nu = \frac{\sinh \alpha(h-h')}{\sinh \alpha h}$$

$$\nu' = \frac{\cosh \alpha h - \cosh \alpha(h-h')}{\sinh \alpha h}$$

Approximations:

i) wide stream ($b \gg h$): $$\frac{\nu'}{\nu} = \frac{\alpha h'(2h-h')}{h-h'}$$

Table 3 - continued

ii) narrow stream ($b \ll h$): $\frac{\nu'}{\nu} = e^{\alpha h'} - 1$

D and E: Effect of variations in third dimension:

$\frac{\partial \phi}{\partial x}$ reduced by $[1 + (\frac{2a}{L})^2]^{-1}$

L = length scale of current

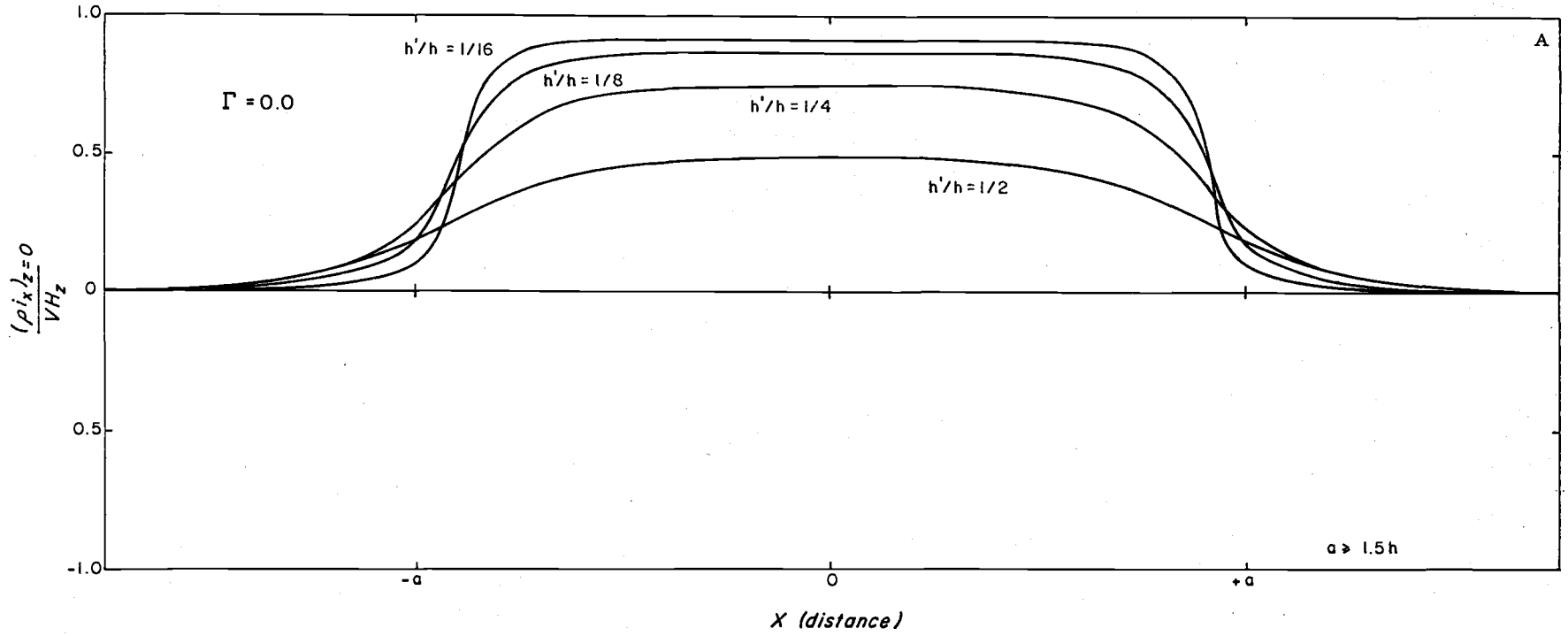

Figure 1. Solutions for a rectangular current that is wide compared to the depth

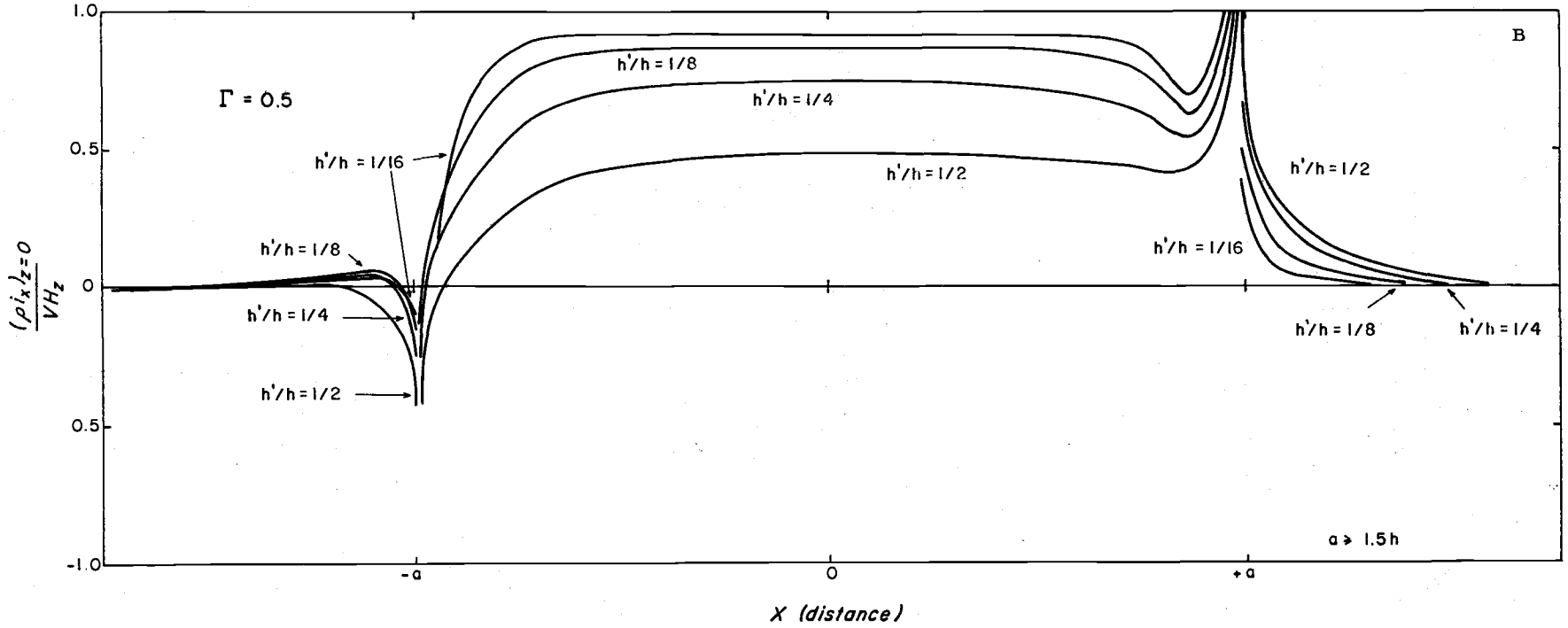

Figure 1. (continued)

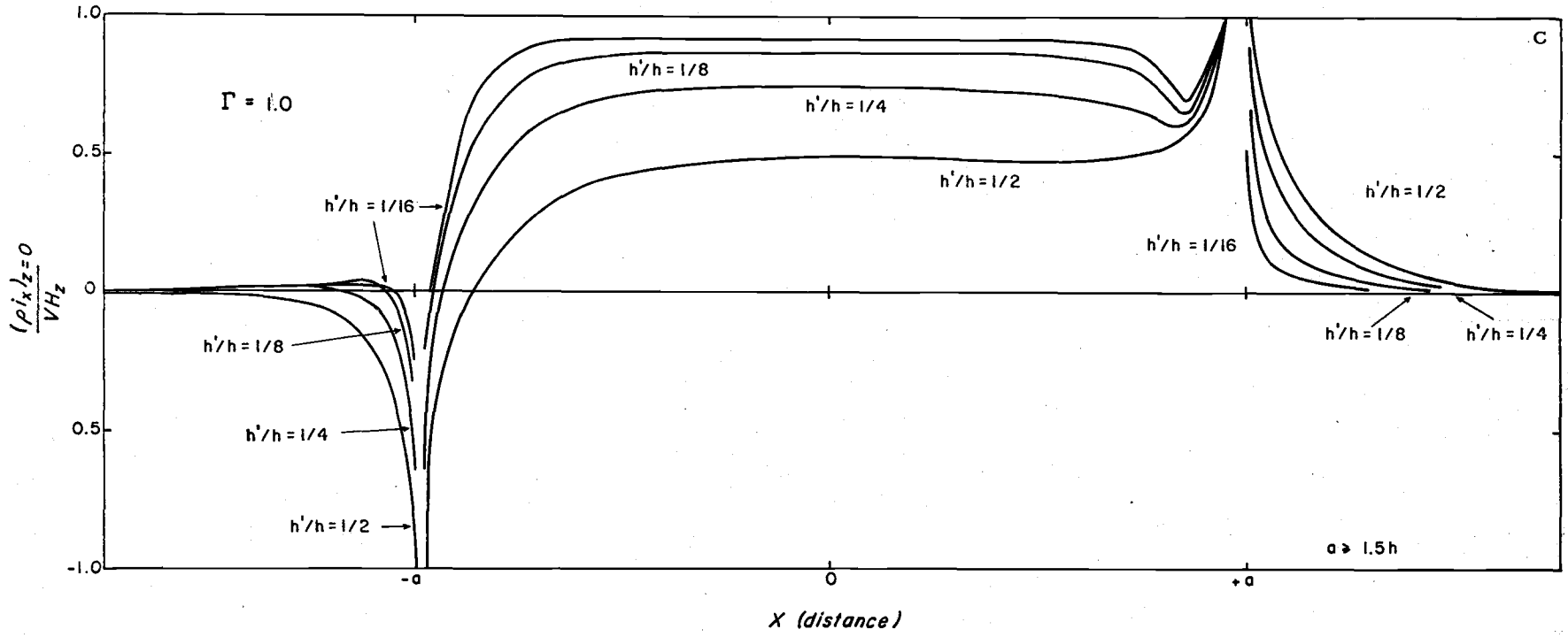

Figure 1. (continued)

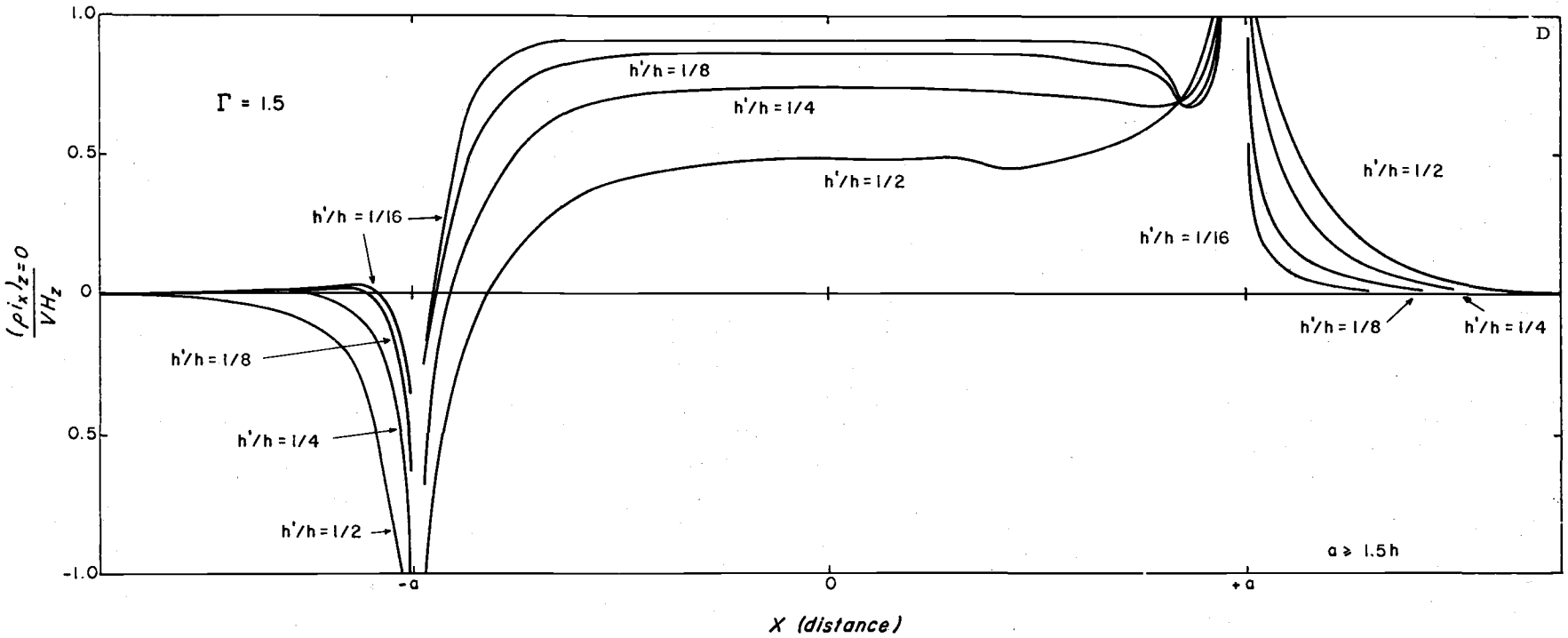

Figure 1. (continued)

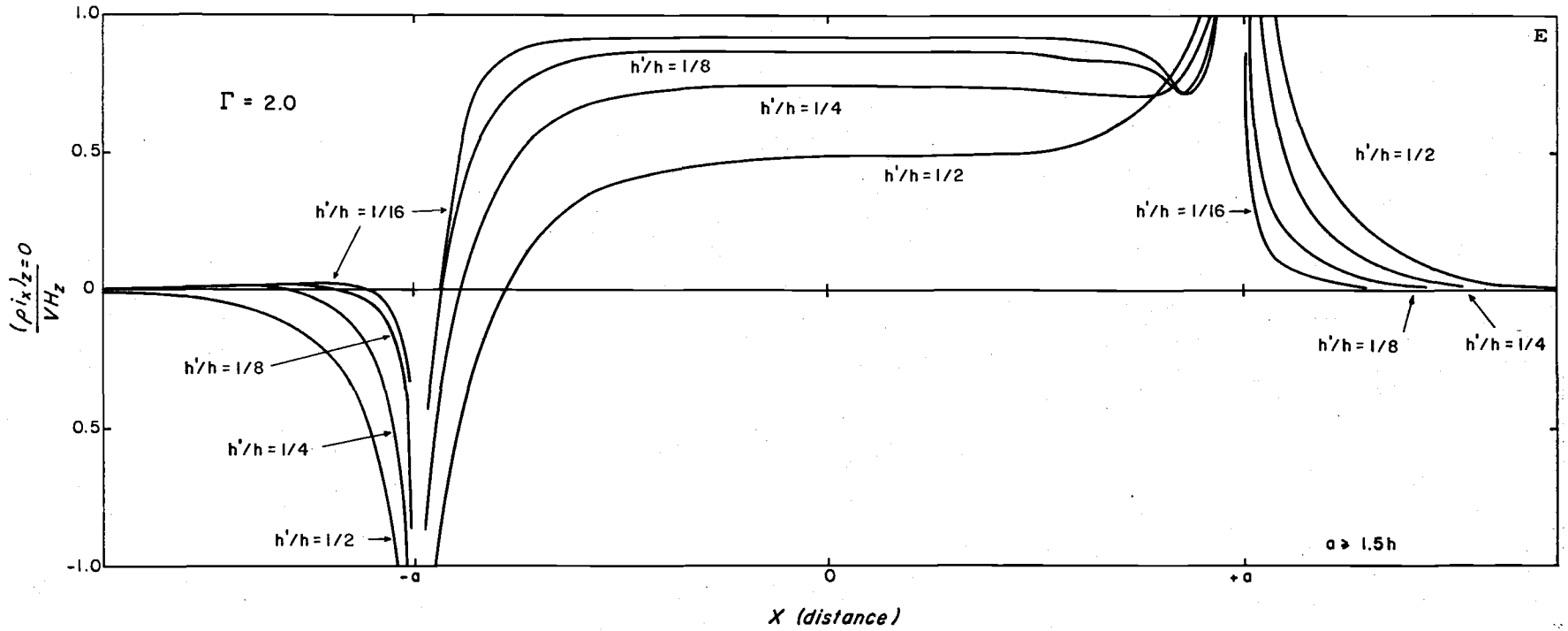

Figure 1. (continued)

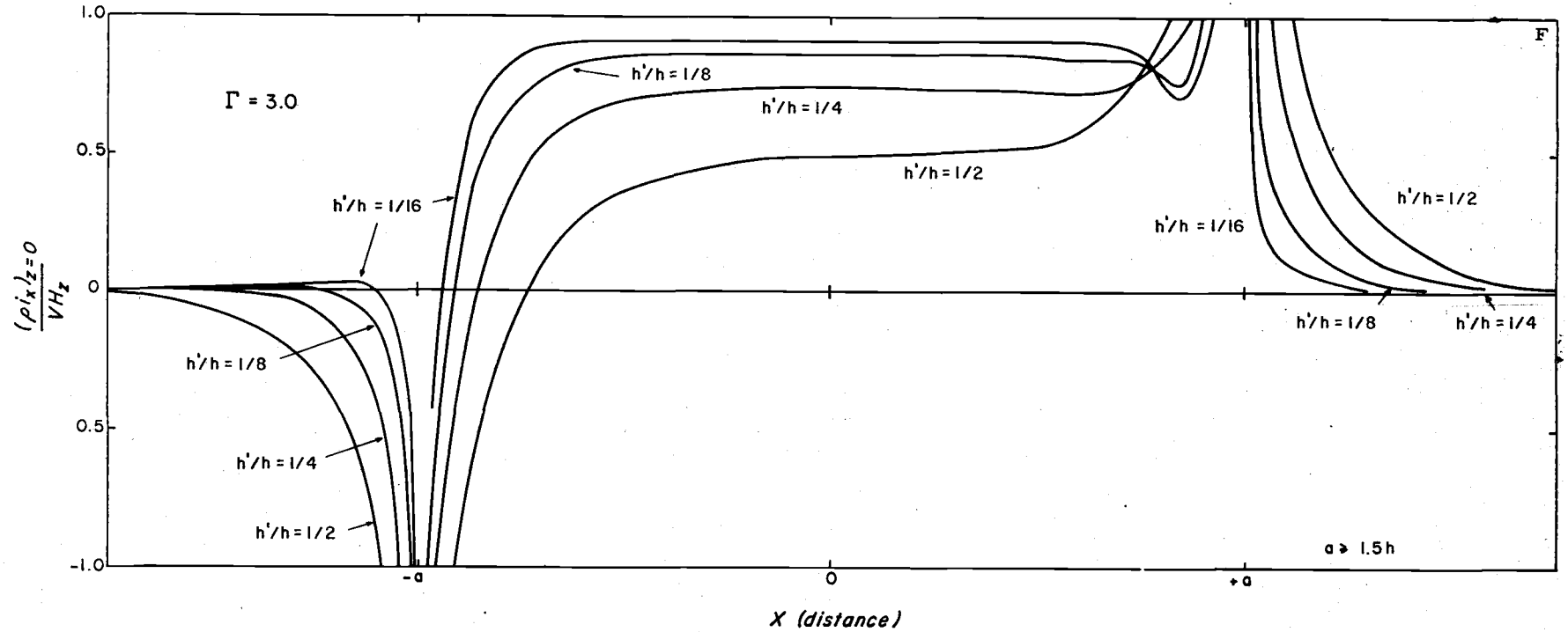

Figure 1. (continued)

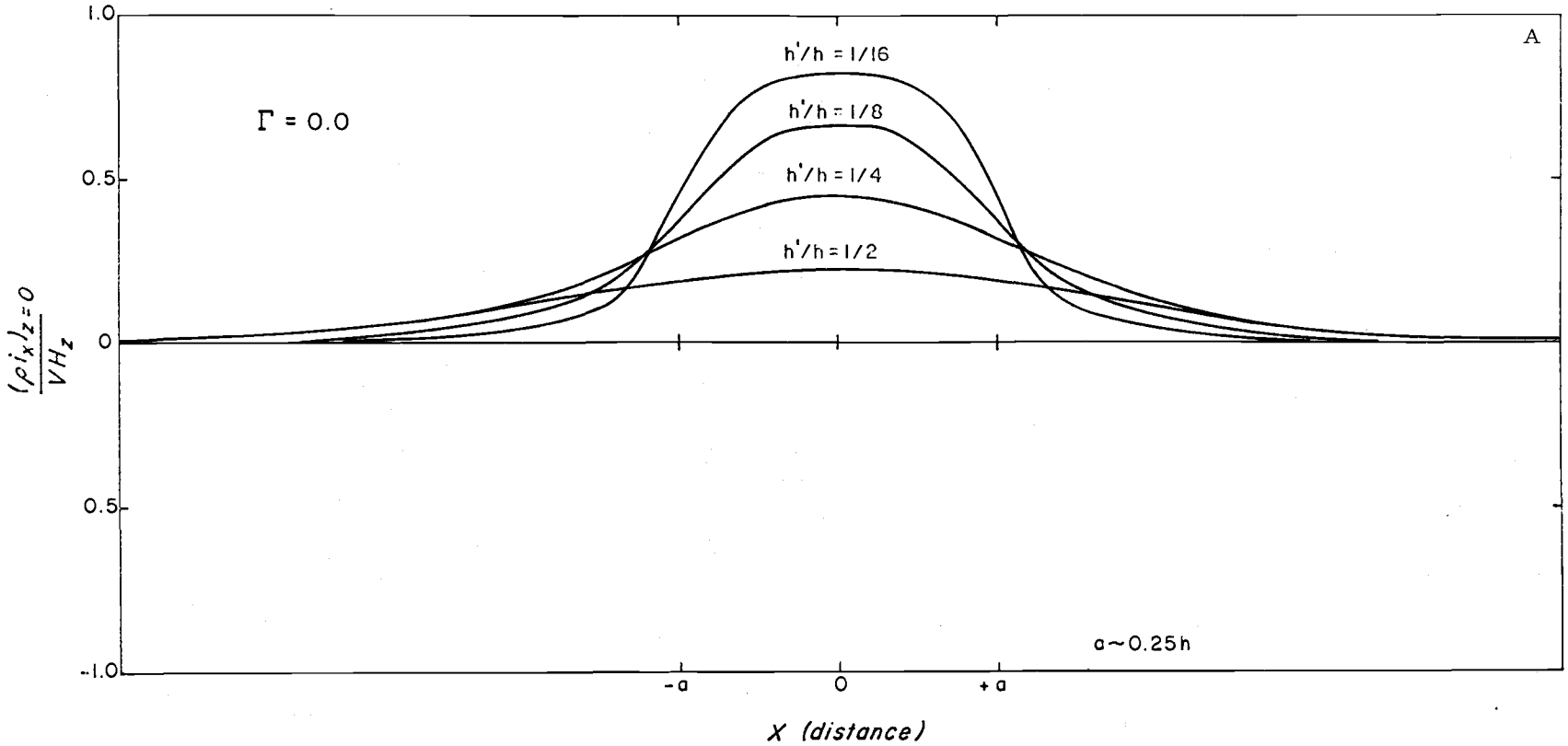

Figure 2. Solutions for a rectangular current that is narrow compared to the depth

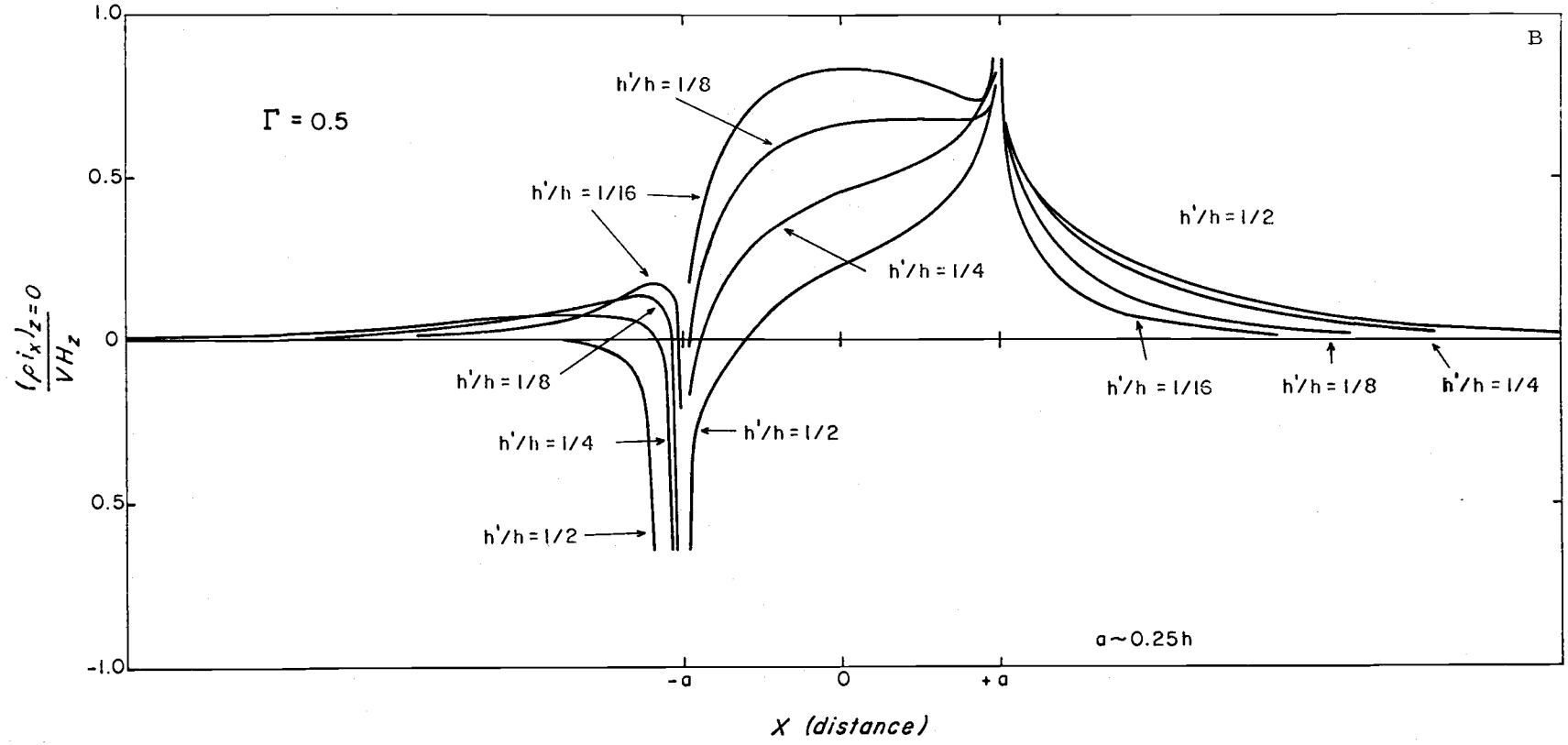

Figure 2. (continued)

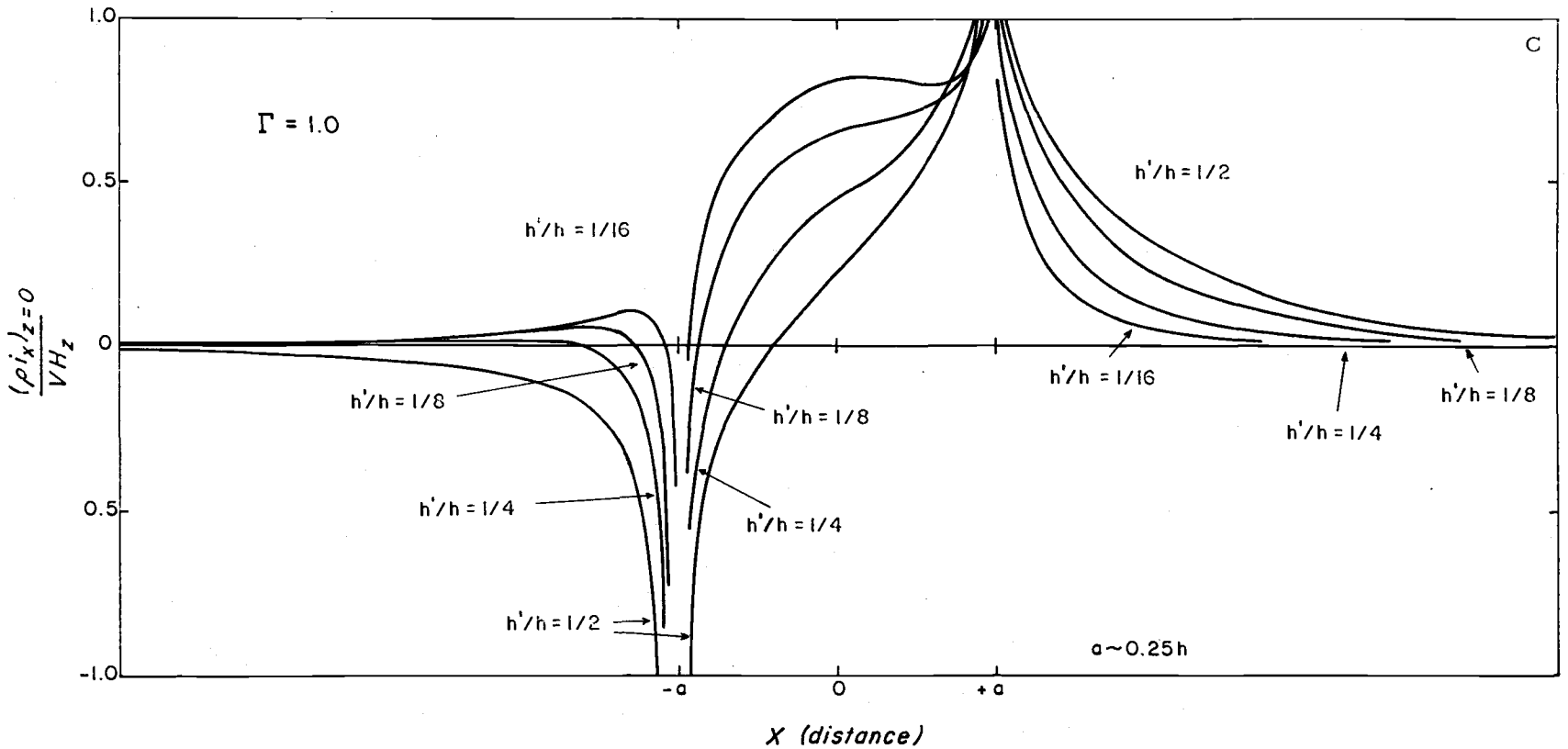

Figure 2. (continued)

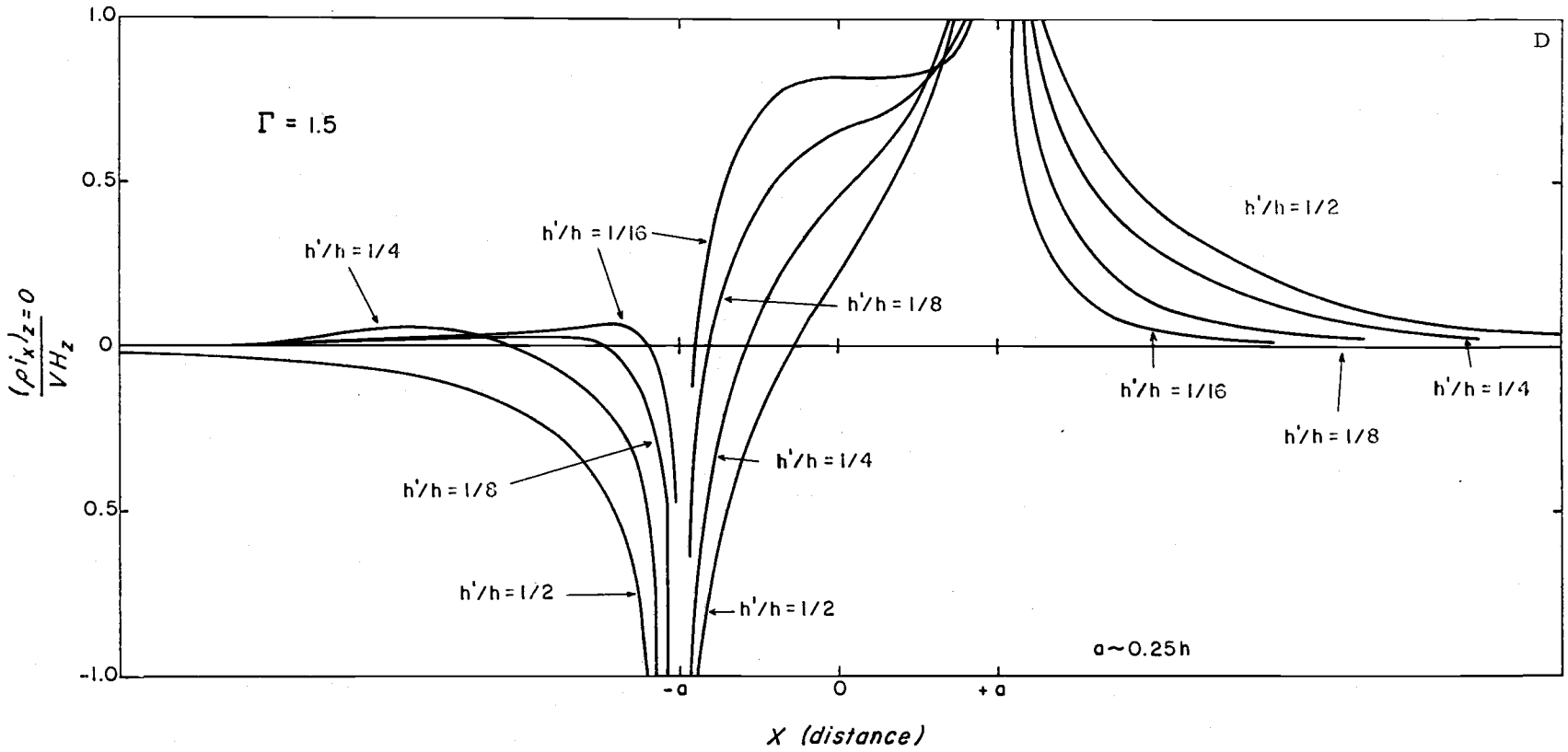

Figure 2. (continued)

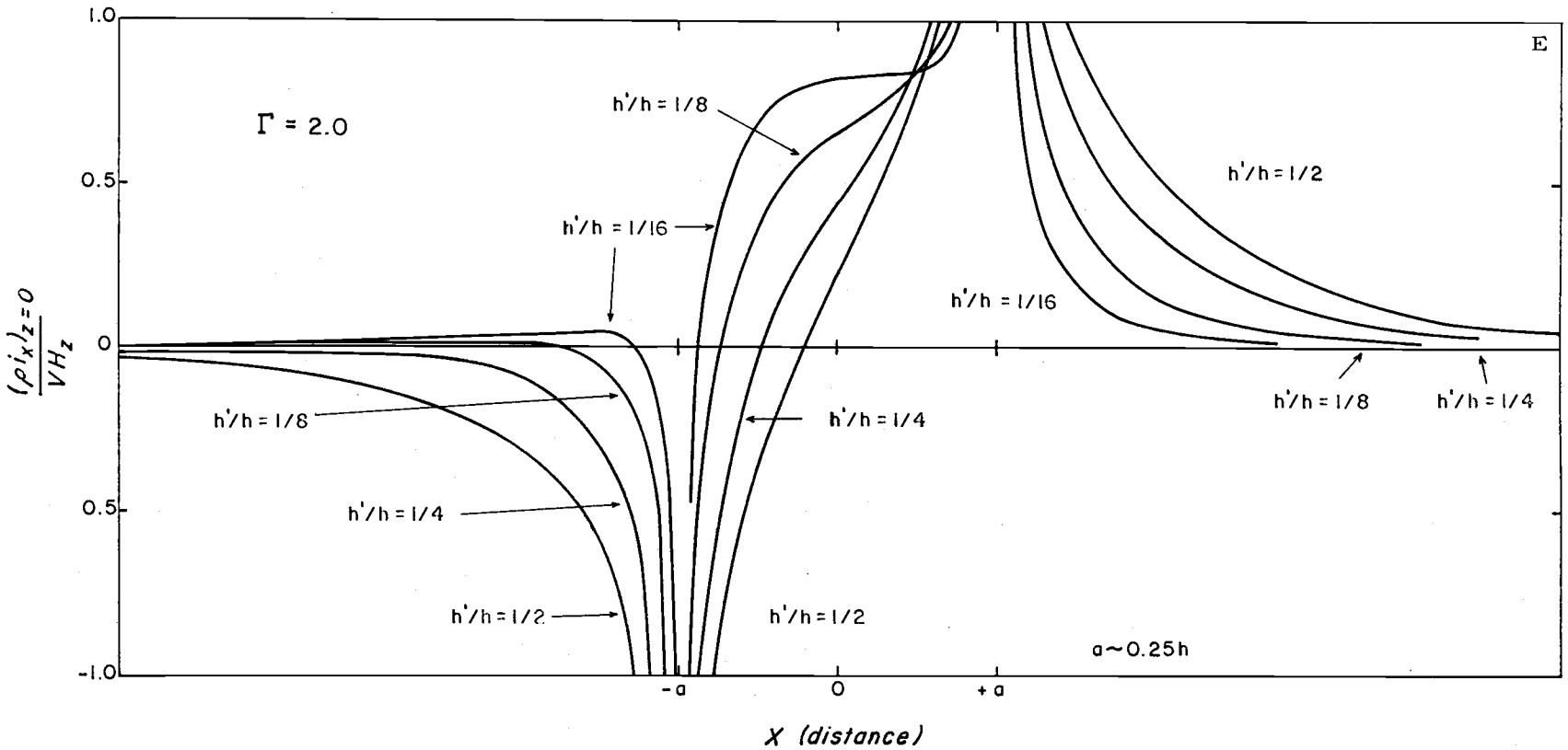

Figure 2. (continued)

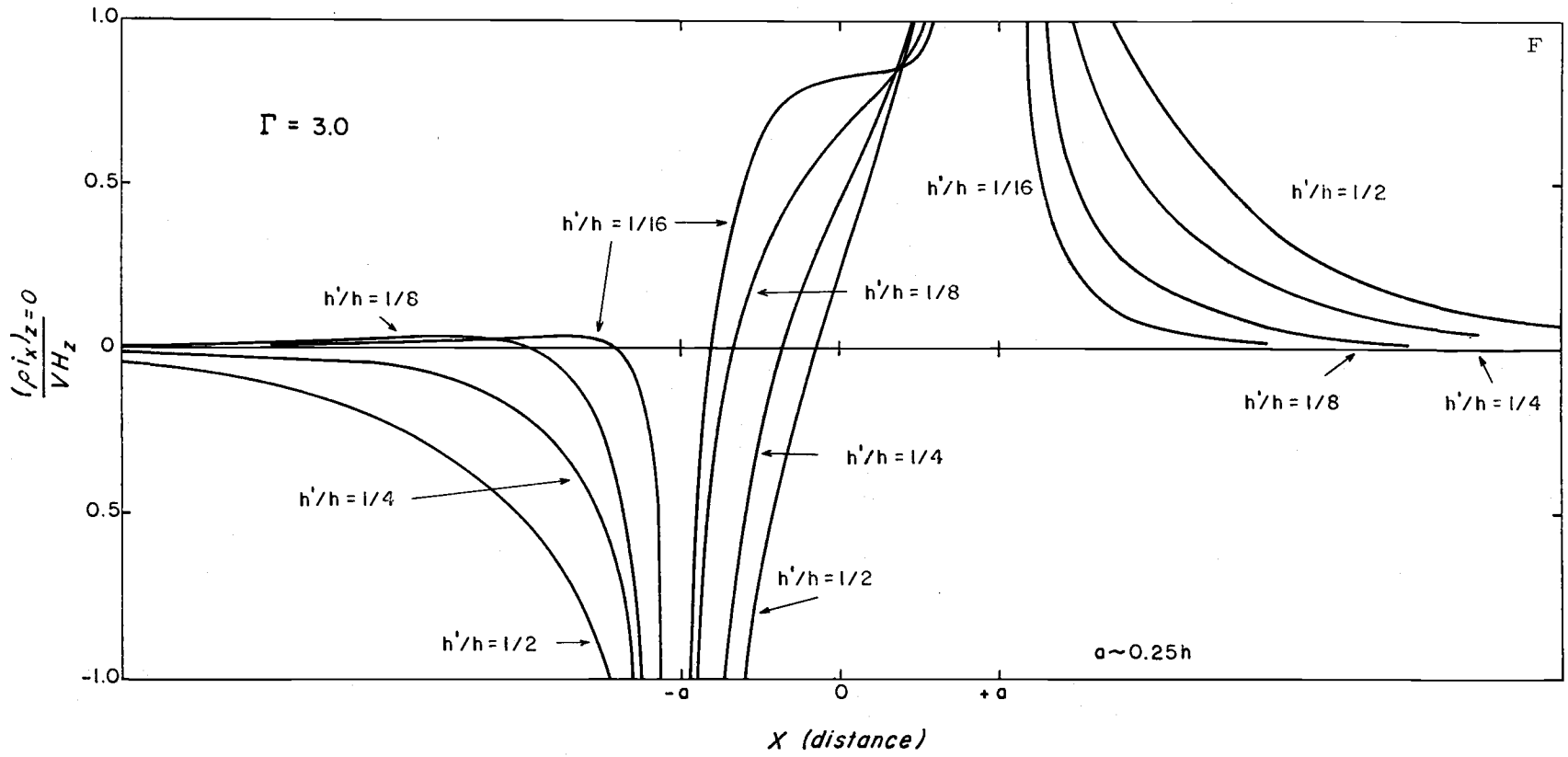

Figure 2. (continued)

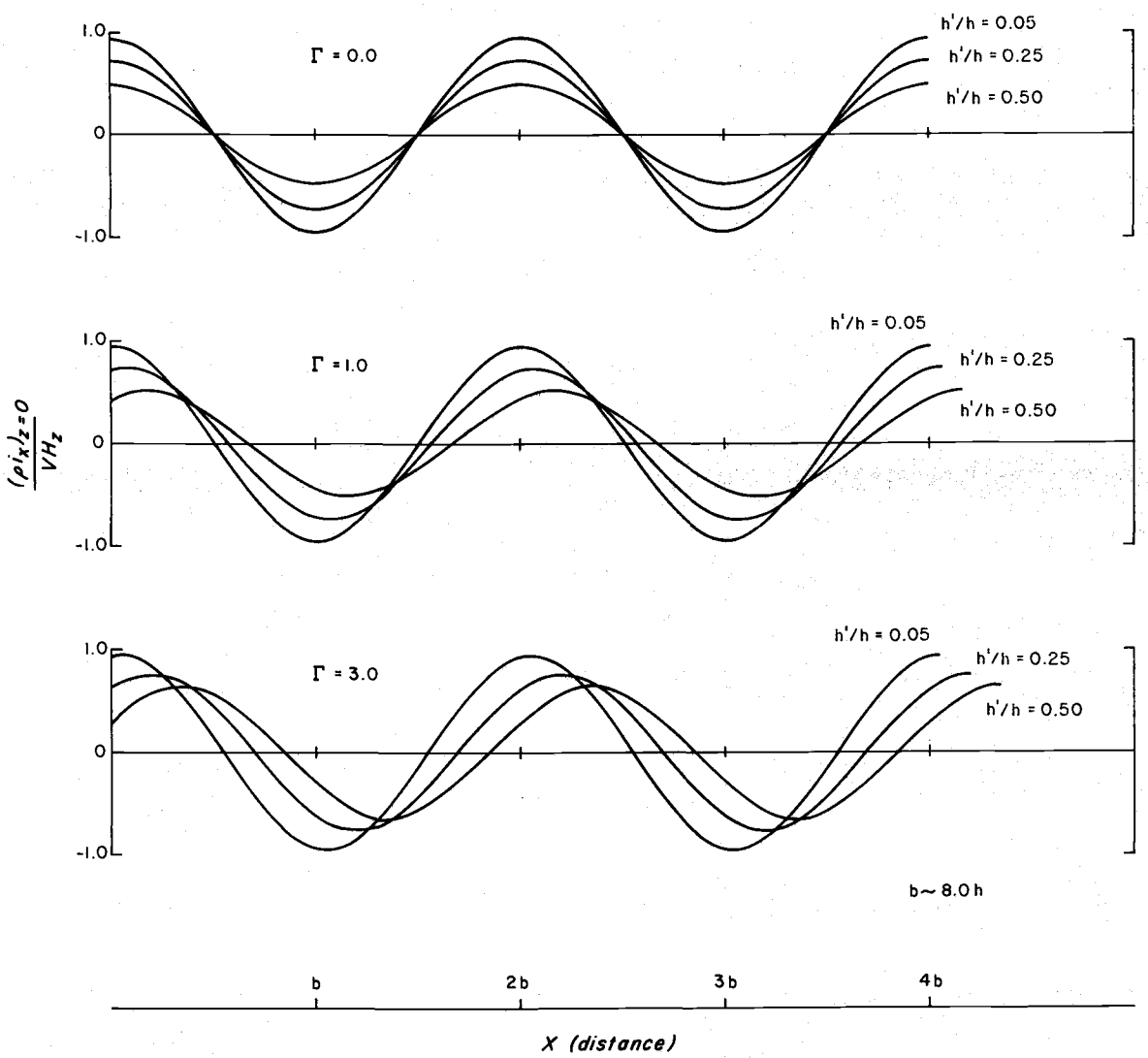

Figure 3. Solutions for a periodic current that is wide compared to the depth

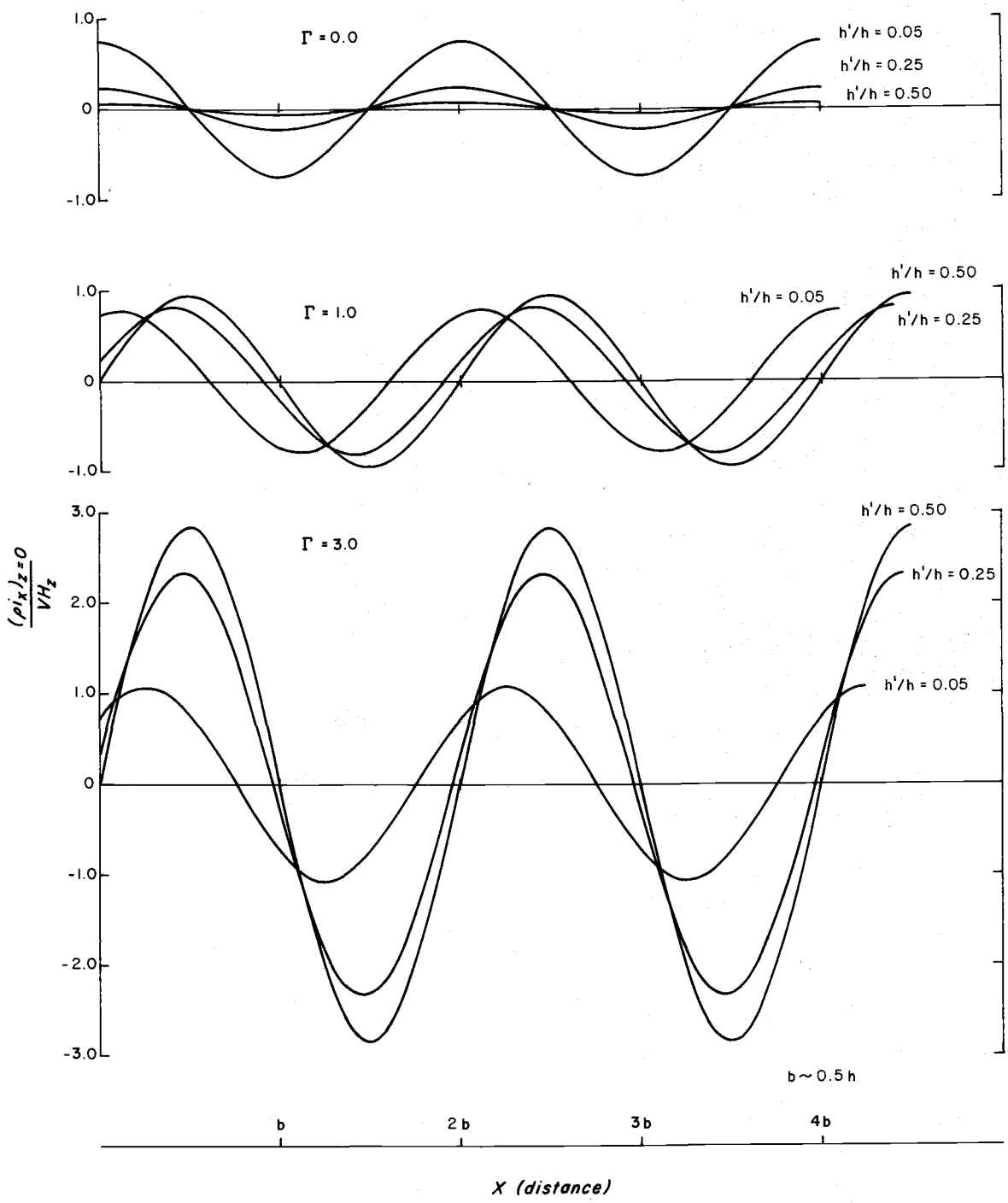

Figure 4. Solutions for a periodic current that is narrow compared to the depth

D. A Suggested Technique for Interpretation of GEK Records

If the recorded signal on the voltmeter ($\int_B^C (\rho i_x)_{z=0} dx$) is divided by the distance between electrodes and by the local vertical geomagnetic field component, the resulting quantity is $(\rho i_x)_{z=0} / H_z$. If this quantity is plotted against distance traversed and the velocity structure was, say for an ideal example, of rectangular shape (of "thickness" h') and wide compared with the depth, h, then the resulting curve would have the same shape as one of the family of curves in Figure 1, where the particular part of the figure used (A, B, ..., F) is determined by the local value of Γ. The data curve still has to be normalized in magnitude to the values on the figure ordinate scale, however, and, as shown on the figures, this normalizing factor is V, the stream velocity. Thus, by matching curve shapes for this ideal case a value of h'/h is found. This gives the thickness h' of the current, since the water depth (h) is known by independent means. Once a particular solution curve in Figure 1 is selected, it is simple to find a normalizing factor to make it and the data curve coincident. This factor is the velocity within the "thickness" determined. This procedure can be followed with any of the four models plotted in figures 1 through 4. Of course, the actual data curves will not look ideally like the plotted solution curves, but a best fit can be approximated.

One previously common interpretive procedure, originally

proposed by von Arx (1950), is to assume a value for h'/h before even looking at the data. The velocity can then be calculated readily by simply dividing the measured signal by the vertical geomagnetic field component and the electrode separation distance, and then multiplying the result by the factor assumed. This factor is called the "k factor" and is defined as $VH_z/(\rho i_x)_{z=0}$, that is, the inverse of the ordinate values in figures 1 through 4. Assuming this factor to be a certain value is equivalent to defining a point on the ordinate in one of the figures, and this, in turn, defines a particular h'/h curve at any point along the distance traversed (abscissa). 1.04 has been suggested by von Arx (1950) as the "k" factor to be used in the open ocean. For a wide rectangular stream model, this corresponds to h'/h of about 0.016 or a current "thickness" of about 60 meters, assuming the depth to be 4000 m.

This method of analysis seems to be rather incomplete in that it takes as assumptions certain facts that should be deduced from the data, namely, the relative depth of the current, of which the measured current speed is a function. As a more rational approach to the method of towed electrodes, the following interpretative technique is suggested whenever possible:

a) Obtain continuous GEK data from the interior of a current, over the "edge" of a current and out into a region where the current is appreciably diminished. To avoid guess-

work regions of high current gradient ("edges") should be covered thoroughly. Figures 1 and 2 show especially that the meaningful interpretation of any GEK measurements using these models depends particularly on what lateral section of the current has been investigated. If the only traverses made were near the center of the current, it would be difficult to distinguish between any one of the four curves in the figures, since they are all essentially horizontal near the center.

b) Plot the data on a graph using distance for the abscissa and the measured signal divided by the vertical component of the geomagnetic field for the ordinate. A smooth curve should be best fitted through the data points by an appropriate averaging technique.

c) Determine ($\Gamma = H_x/H_z$) for the geographic location.

d) Compare the empirical plot to the graphs in figures 1 through 4 for the appropriate value of Γ, and select a theoretical solution curve which best represents the "shape" of the data curve.

e) The selected solution curve will thus indicate the depth of the current stream relative to the total depth (h'/h). The constant by which the empirical curve must now be divided to make it coincident with the theoretical one is

then the velocity within the indicated current stream.

In comparisons of these forms with actual data, one must bear in mind that the measured signal may have been increased by two further effects. First, variations of the water velocity in the third dimension will tend to reduce the potential gradient by allowing electrical currents to flow in the horizontal plane. Sanford (1967) estimated this effect and it is listed in Table 3. Second, the bottom has been assumed to be non-conducting in the graphically illustrated solutions. Finite conductivity will increase the electrical currents present, especially for "thick" currents. Both Longuet-Higgins, Stern, Stommel (1954) and Sanford (1957) have considered cases of finite bottom conductivity. Their results indicate that this effect is unimportant for baroclinic currents in the deep ocean. Bottom conductivity is important, however, for barotropic flows as demonstrated by Larsen (1966) in an analysis of tidal effects. Hughes (1962) concluded that local bottom conductivity is the dominant factor controlling the magnitude of electrical currents over areas of shallow water. Thus the suggested technique above is primarily for use in considering baroclinic currents in the deep ocean.

III. TIME-DEPENDENT EFFECTS

A. General

As has been discussed, the motion of sea water through the earth's magnetic field produces potential differences, and these in turn cause electric currents to flow. These currents are a direct function of the electrical characteristics of the local environment, and their magnitudes determine the signal measured by towed electrodes. However these currents also induce two further effects.

First, the currents themselves produce a magnetic field which then interacts with the initial field of the earth and may thus modify the earth's field. These are electromagnetic effects. Second, the currents flowing within the geomagnetic field produce a body force (Lorentz force) which alters the fluid flow. These are hydromagnetic effects. Both effects together form the subject of magnetohydrodynamics. Reference is made here to Roberts (1967) whose notation is adapted throughout this chapter.

For a steady-state velocity field these effects are uninteresting in that they are undetectable. But for time-dependent flow these effects may or may not be dynamically significant, depending upon the physical conditions involved. Since the method of towed electrodes is essentially based on the current density generated, it seemed instructive to estimate the electromagnetic and hydromagne-

tic effects of this current for oceanic variables. Table 4 defines the terms, and Table 5 lists sea-water values used in the calculations.

B. Electromagnetic Effects

The magnitude of the induced field relative to the geomagnetic field can be estimated by the value of the magnetic Reynolds number (R_m). If R_m is of order 1 or greater the geomagnetic field is significantly affected by the magnetic effects of the fluid motion. As shown in Figure 5-A, small-scale motion of almost any magnitude in the ocean does not produce large effects. Figure 5-B demonstrates, however, that the earth's field is affected significantly by larger-scale flows in the order of tens of kilometers in length (see, for example, Larsen, 1966). In general, it is seen that for velocities found in the ocean, electromagnetic effects are unimportant for length scales of steady motion less than 100 kilometers.

For time dependent variations, Sanford (1967) has shown that $\partial \vec{A}/\partial t$ can be neglected in the field equations provided the horizontal scale of the time-dependent component of flow is small compared to the electromagnetic skin depth. Figure 5-C plots the skin depth as a function of the time characteristic of a given disturbance. For example, a velocity fluctuation with a period of two hours would be significant electromagnetically if it were greater than 40 kilometers

Table 4. Definitions of Terms

η	$= (\mu g)^{-1}$	= magnetic diffusivity
V'	$= B(\mu \rho_o)^{-1/2}$	= Alfvén velocity
A	$= U/V'$	= Alfvén number
R_m	$= UL/\eta$	= magnetic Reynolds number
Lu	$= V'L/(\eta+\nu)$	= Lundquist number
M	$= V'L/(\eta\nu)^{1/2}$	= Hartmann number
p_m	$= \nu/\eta$	= magnetic Prandtl number
τ_A	$= L/V'$	= Alfvén travel time
τ_η	$= L^2/\eta$	= electromagnetic diffusion time
τ_m	$= \eta/V'^2$	= magnetic response time
d_η	$= (\eta T)^{1/2}$	= electromagnetic penetration depth
d_A	$= V'L^2/(\eta+\nu)$	= hydromagnetic penetration depth
d_h	$= (\eta\nu)^{1/2}/V'$	= Hartmann depth

Table 5. Average Oceanic Values

ν = 1.3×10^{-6} m^2/sec

ρ_o = 1030 kg/m^3

μ = 1.0×10^{-6} n/amp^2

g = 4.0 mho/m (at T $\approx$ 13°C, S $\approx$ 35‰)

H = 0.5 oersted $\approx$ 40 amp/m

B = 4.0×10^{-5} $weber/m^2$

η = 2.5×10^{5} m^2/sec

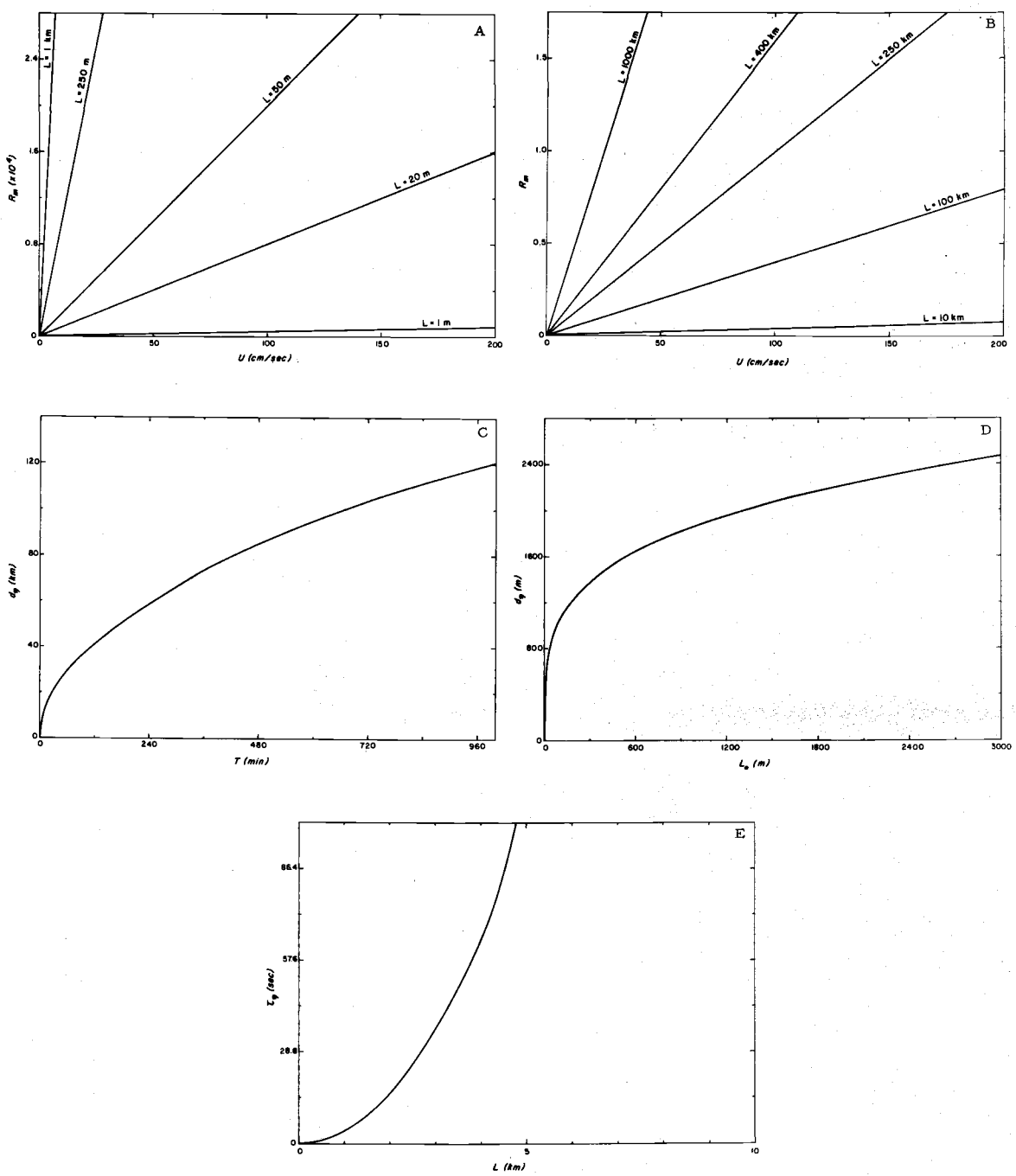

Figure 5. Electromagnetic characteristics as functions of parameters of oceanic scale. See text for details.

in scale. Another case is illustrated by Figure 5-D where the deep-water wave length is related to the skin depth. It is seen that gravity waves (deep water) less than 2000 meters in length do not produce important electromagnetic effects. For any particular regional velocity effect, Figure 5 can be used to estimate the influence of the induced magnetic fields.

The electromagnetic diffusion time (τ_η) is plotted as a function of the length scale in Figure 5-E. This factor is of heuristic interest in that it gives the time necessary for ohmic losses to dissipate the energy change caused by the fluid moving across the field. Thus in the deep ocean, energy changes induced by motion of a scale comparable with the depth are dissipated in about 1 minute.

C. Hydromagnetic Effects

The extent to which the velocity field is affected by the induced magnetic field can be determined by the value of the Alfvén number (A). This essentially is the ratio of the velocity field strength to the magnetic field strength. If $A \gg 1$, the velocity field is little affected by the magnetic field, and kinetic stresses far outweigh magnetic stresses. Figure 6-A shows that the field of motion in the sea is little affected by the magnetic effects associated with the induced current density.

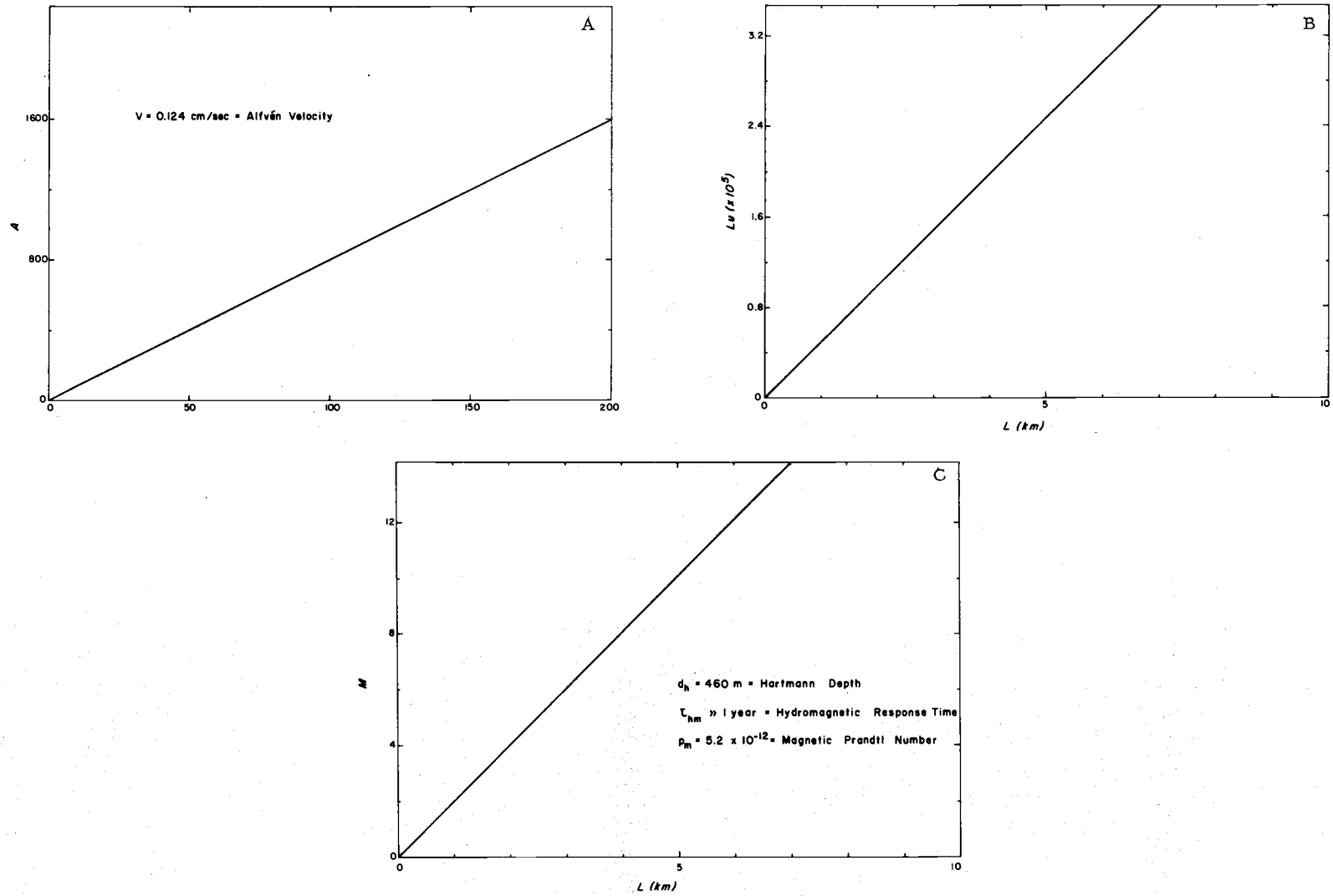

Figure 6. Dimensionless hydromagnetic numbers as functions of parameters of oceanic scale. See text for details.

More explicitly, hydromagnetic disturbances can be divided into two characteristic components (see Roberts, 1967): a k_1 mode (Alfvén wave), and a k_2 mode. The importance of Alfvén radiation (k_1 mode) in any situation can be judged by the value of the Lundquist number (Lu). For values of Lu $<<1$, any excited Alfvén waves are attenuated within a short distance relative to the system under consideration. Figure 6-B shows that this mode is insignificant in the ocean.

k_2 disturbances are largely confined to a layer equal in thickness to the Hartmann depth. This depth is about 460 meters in the ocean. The effect is rendered unimportant, however, because its magnitude contains a factor called the magnetic Prandtl number, which is of order 10^{-12} in the sea.

Thus for the two hydromagnetic modes in the ocean, Alfvén radiation is readily generated yet rapidly attenuated, whereas k_2 radiation has a significant propagation distance, but its efficiency of generation is so small that its effect is negligible.

Figure 6-C illustrates the relative sizes of dissipative forces for oceanic length scales. The Hartmann number (M) is the ratio of the magnetic drag to the viscous drag. For variations greater than 1 kilometer in scale, the magnetic drag dominates over the viscous drag as a mechanism of energy dissipation. That this process is not a significant energy sink is emphasized by the hydro-

magnetic response time (τ_{hm}). τ_{hm} reflects the time necessary for the hydromagnetic field in the ocean to dampen out an initial fluid motion. It is of the order of years for average oceanic parameters. That the magnetic drag is greater than the viscous drag is really only a lower lower bound, since the viscous drag is an extremely small quantity itself.

IV. OBSERVATIONS OF STABILITY OSCILLATIONS

A. Observational Data

During January-February, 1969, the signal from towed electrodes was continuously recorded along tracklines of a cruise to the eastern tropical Pacific Ocean. Hydrographic data was also taken at frequent intervals along the way. Portions of the resulting data exhibited a marked periodicity of order two minutes with amplitude increasing with decreasing latitude. Figure 7 indicates the sections along which this mode of periodicity was noticed in the record. Figure 8 presents examples of part of the actual signal recorded on the passages marked in Figure 7. This signal is shown exactly as it appears on the chart paper with no reference to displacement from the zero point. In otherwords, the periodicity is a perturbation superimposed on the main GEK signal, and it does not indicate the absolute ocean current magnitude. The contention here is that this phenomenon is the electrical field produced by stability oscillations of the thermocline, that is, by the lowest internal wave mode in the ocean. In order to prove this hypothesis, the most pronounced oscillations, shown in Figure 8-C, will be analyzed in detail. Analogous conclusions can be deduced for the remaining observations for which a reduced amplitude can be expected (as will be demonstrated).

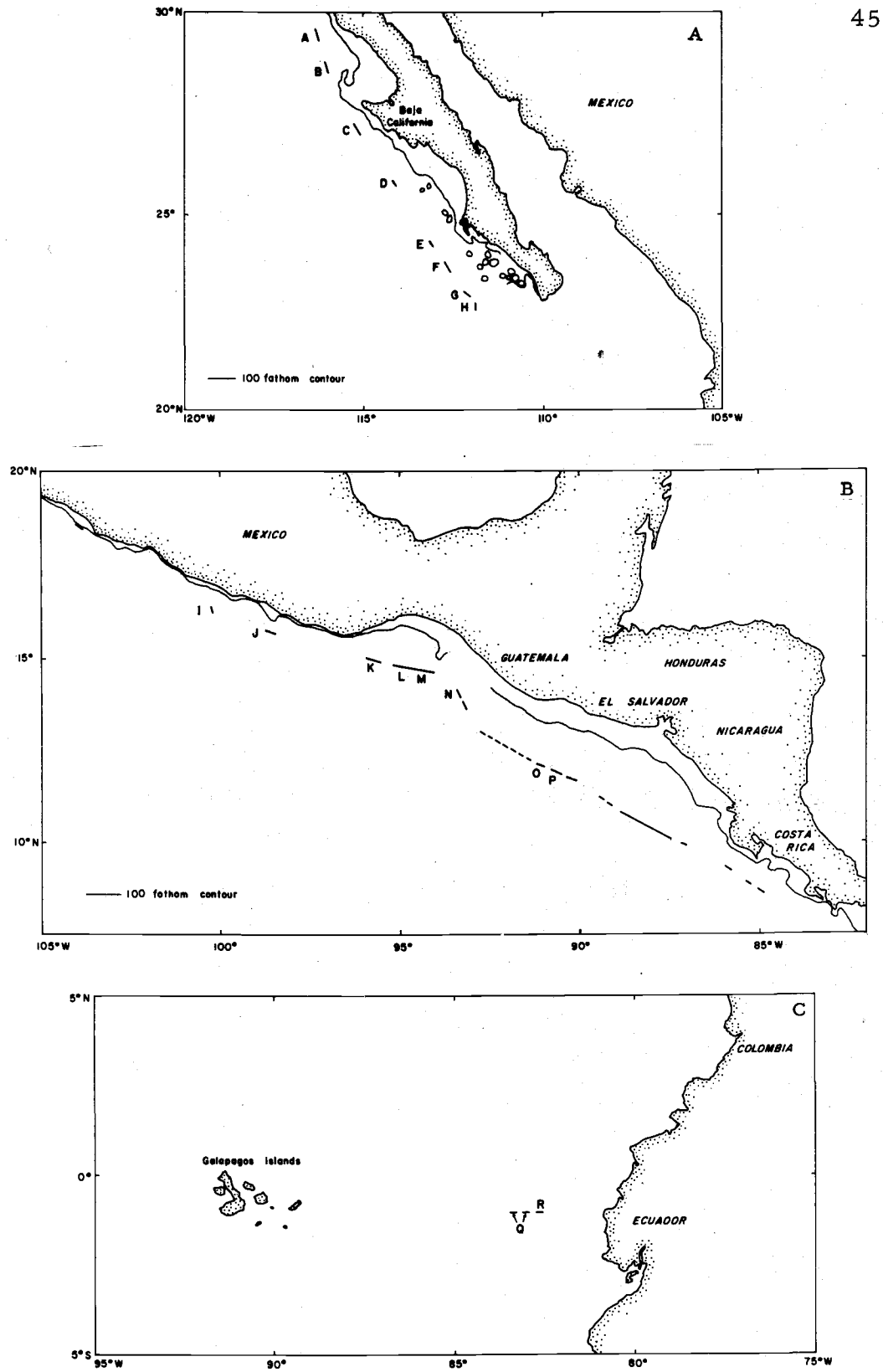

Figure 7. Lines along which oscillations of two minute order were observed in the measured signal.

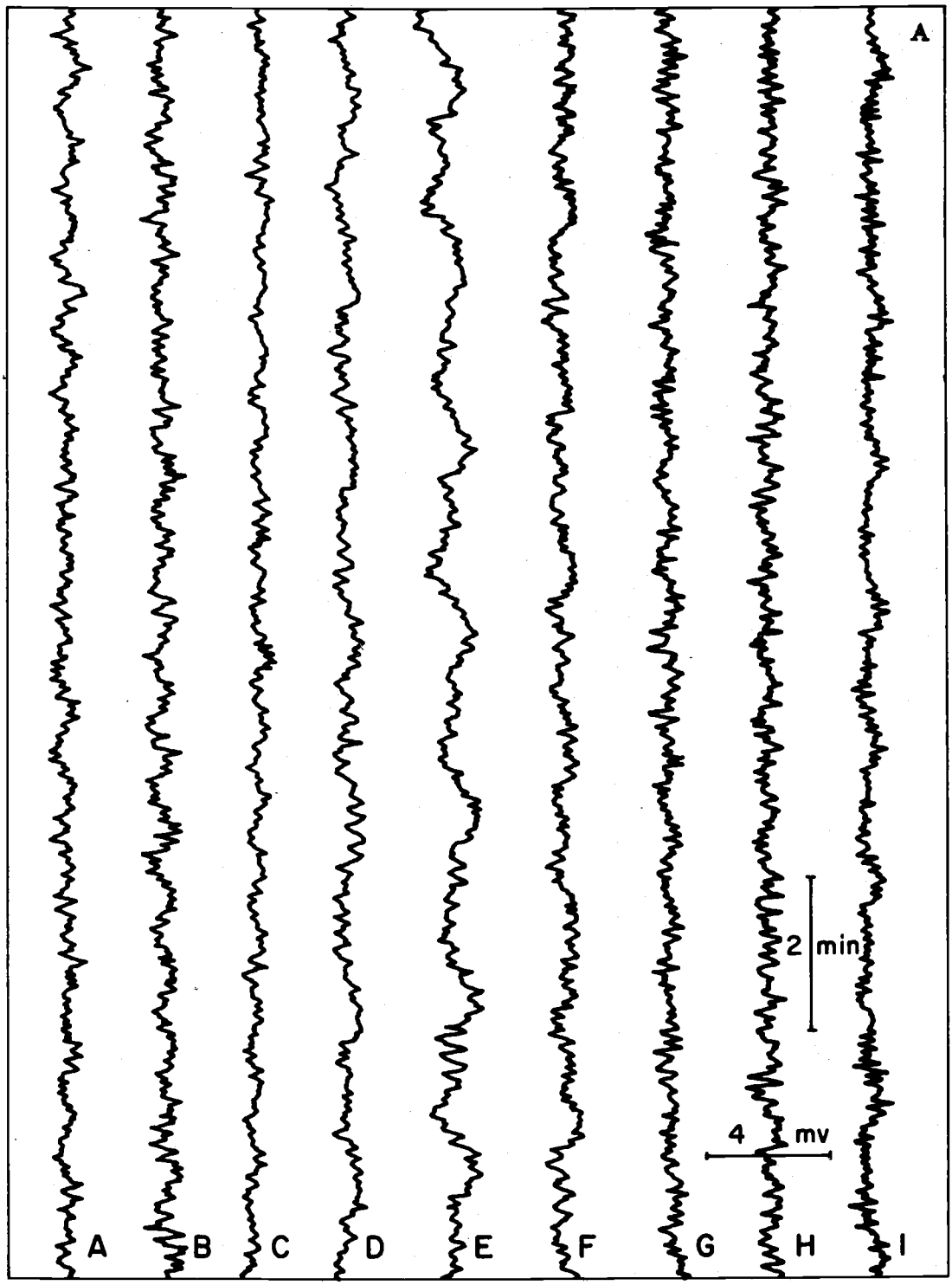

Figure 8. Examples of the type of signal measured by towed electrodes at positions indicated in Figure 7.

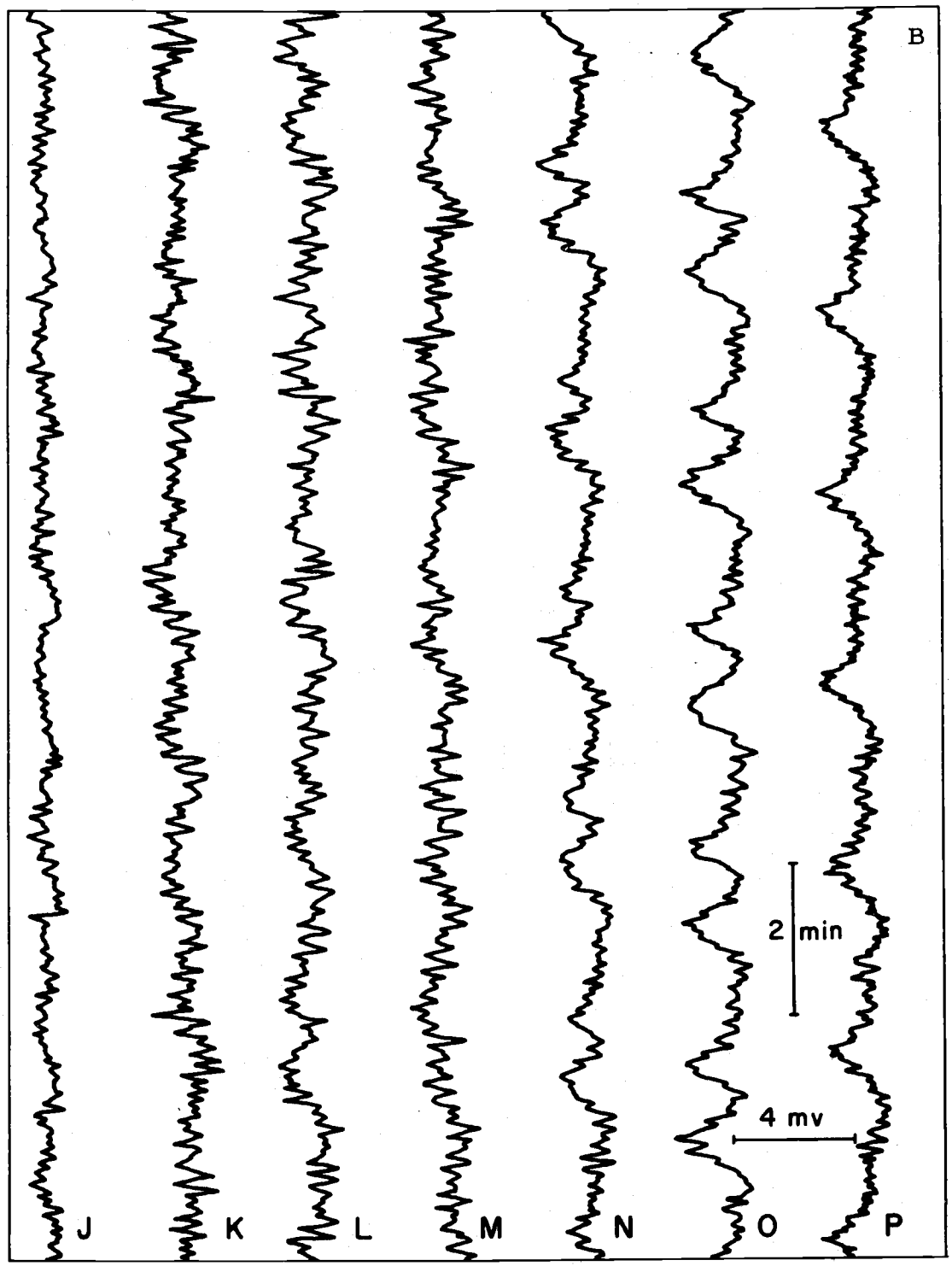

Figure 8. (continued)

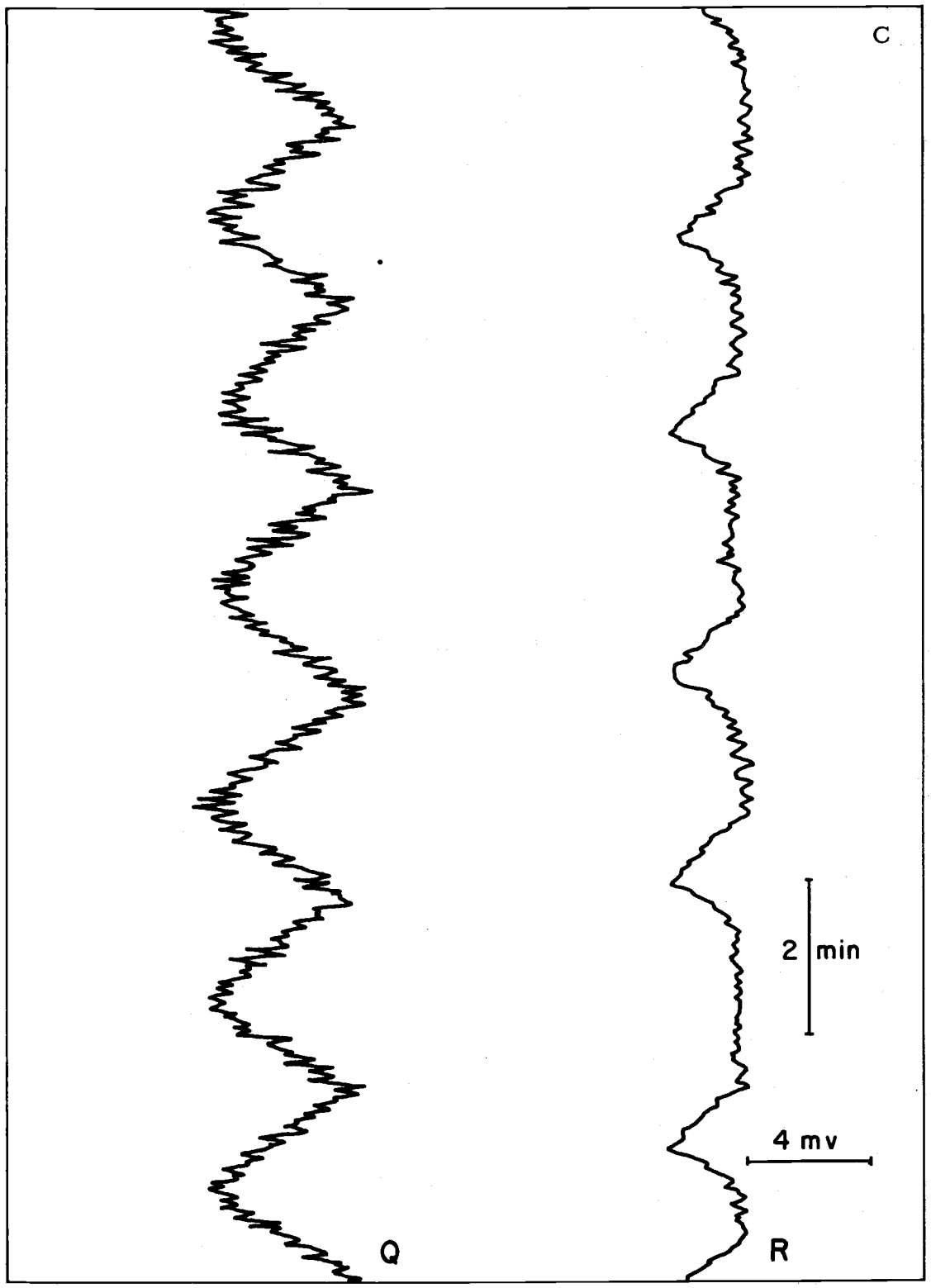

Figure 8. (continued)

B. Specific Analysis

Figure 8-C is a representative example of the signal recorded along the lines indicated in Figure 7-C. These lines are located between stations 63 and 65 on the sections shown in Figure 9. The predominant current component during the traverse across this section was south, that is, toward the reader looking at Figure 9. It is proposed that the observed oscillations are the electrical manifestation of oceanographic "lee waves" (cf. Defant, 2, 1961, page 569) caused by the large ridge in the local bathymetry as seen in the figure. The motion of the wave form is most clearly manifested in the thermocline which heaves up and down periodically. Individual particles trace vertical trajectories similar to those of a standing wave. First, the general characteristics of the waves themselves will be deduced. Second, their existence as lee waves is inferred.

That these oscillatory potential differences were not caused by temperature and salinity variations along the cruise track is shown from the results of Appendix B. Electrochemical potentials are in the order of microvolts for silver-silver chloride electrodes, whereas the observed oscillations here are well into the millivolt range. More important, however, are the periods involved. The large electrochemical lag times shown in Appendix B are not at all consistent with the observed two-minute periods here. Thus, both the amplitude and frequency of the disturbance eliminates oceanic

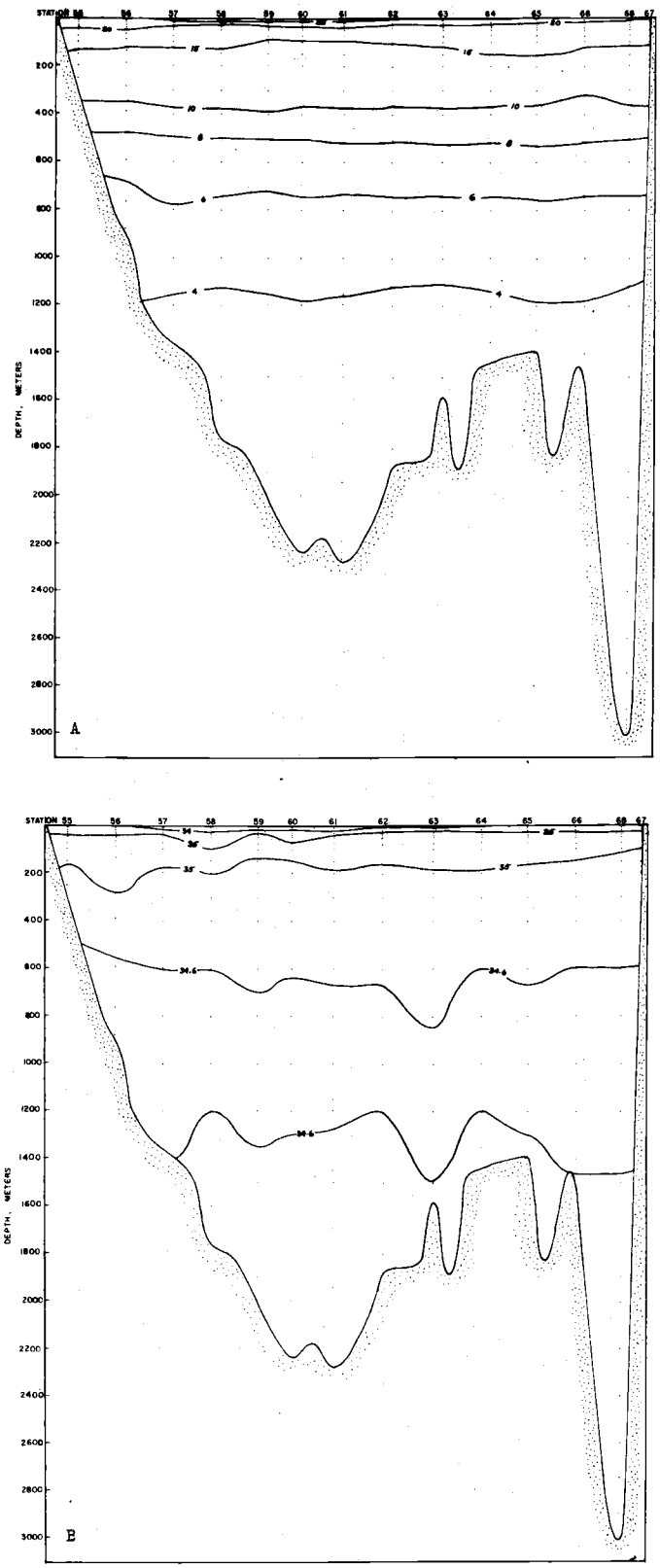

Figure 9. Temperature (A) and salinity (B) sections from the Galapagos Islands to the Ecuadorian coast as shown in Figure 7-C.

temperature and/or salinity variations as contributing any significant emf in this case.

The distribution of the Brunt-Väisälä frequency with depth is plotted in Figure 10 for stations 64, 65 and 61 respectively. The sharp peaks indicate a well developed, shallow thermocline, as expected in the tropics and subtropics. Such a condition is highly conducive to internal wave generation of the first mode (stability oscillations). Phillips (1966) shows that the frequency of this lowest mode in the deep ocean can be written:

$$\sigma^2 = \frac{\delta \rho'}{\rho'_o} \frac{gk}{1+\coth kd} \qquad \text{IV. 1}$$

as long as $k(D-d) \gg 1$, where $\delta\rho'$ is the density difference above and below the thermocline, ρ'_o is the mean surface density, k and σ are the wave number and frequency, respectively, and d is the thermocline depth with D as the total depth. The maximum Brunt-Väisälä frequency $(= (-\frac{g}{\rho'_o} \frac{\partial \bar{\rho}'}{\partial z})^{1/2})$ is thus seen to be a rough indicator of the maximum natural oscillation frequency for a given density field. It is instructive to compare the minimum Brunt-Väisälä periods at Q and R (Figures 10-A,-B) with those observed electrically (Figure 8-C).

	Calculated Period (sec)	Observed Period (sec)
Q	190	160
R	161	165

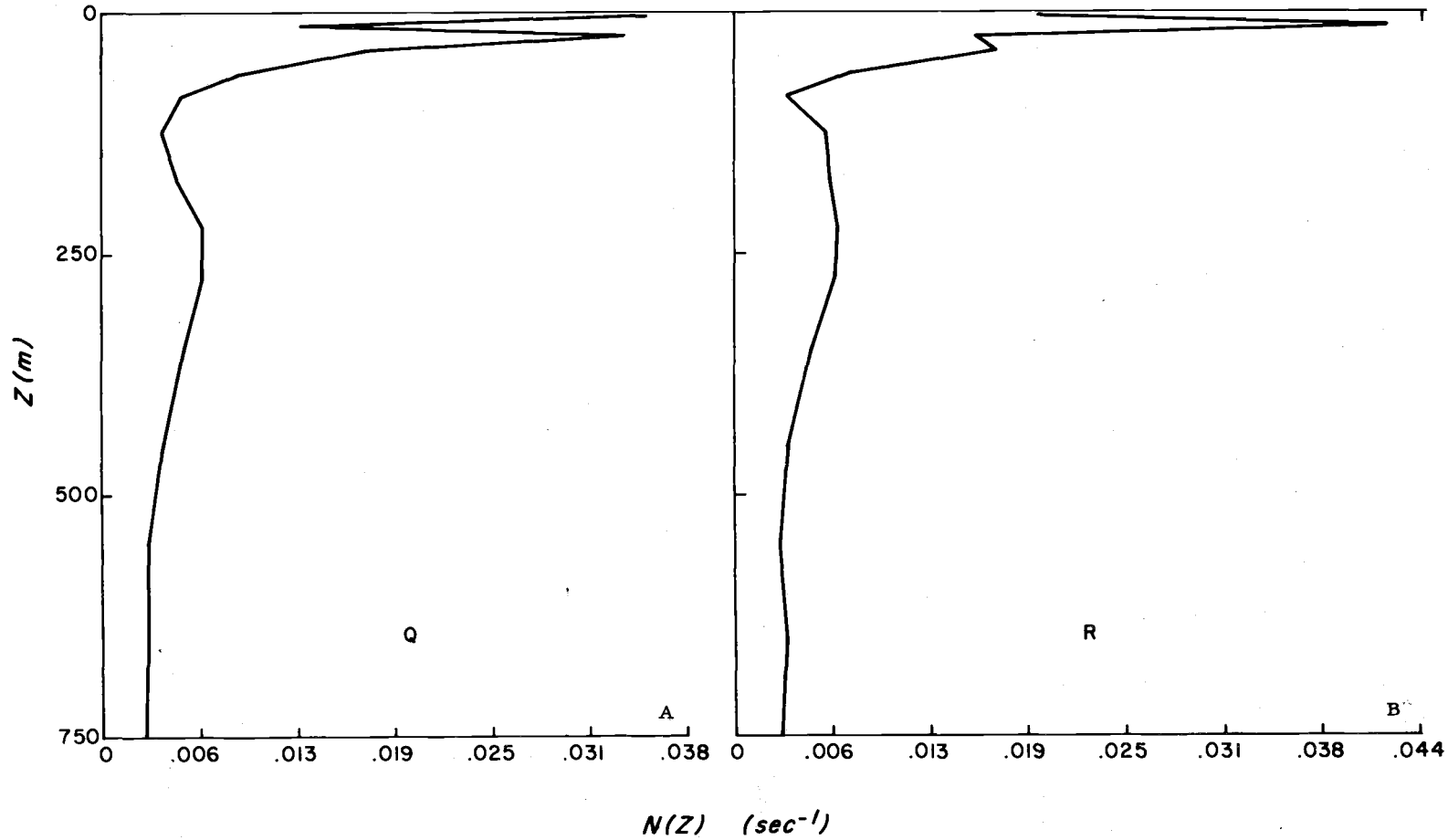

Figure 10. The Brunt-Väisälä frequency as a function of depth for positions indicated in Figure 7.

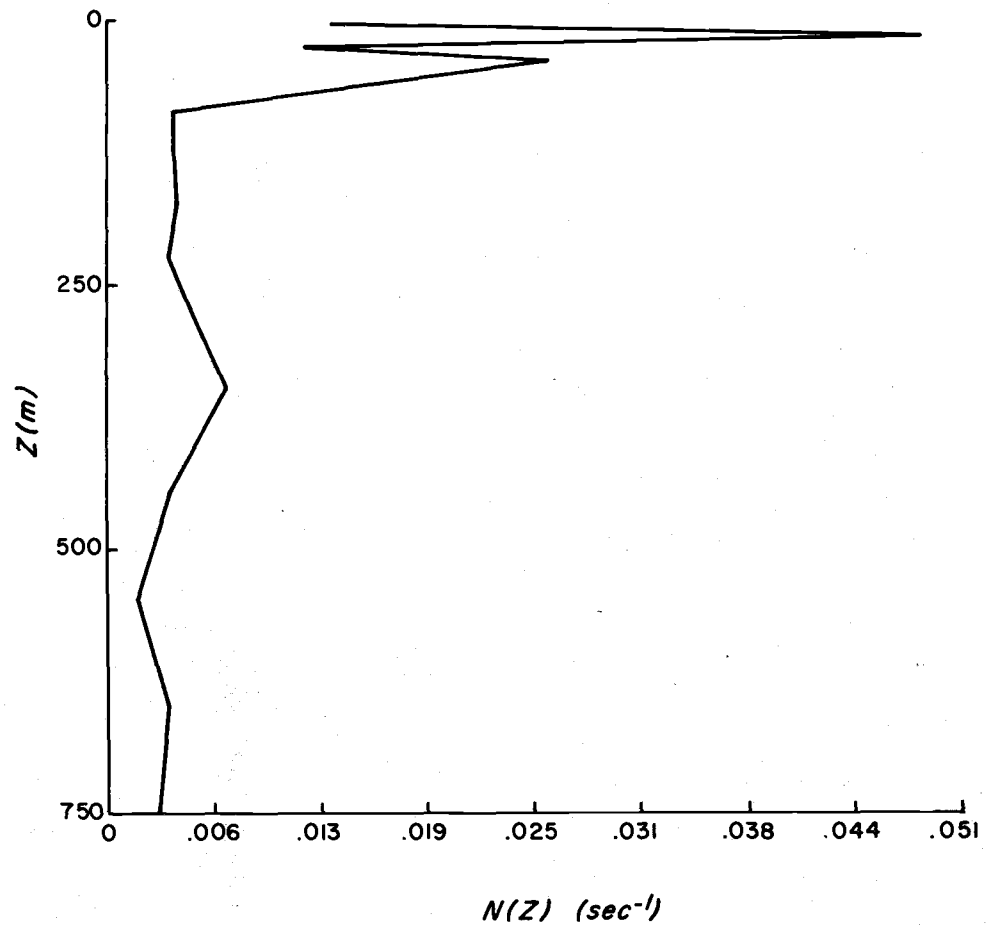

Figure 10. (continued)

If $kd < 1$, which is reasonable for the shallow thermoclines in this region, the wavelength of the disturbance can be readily calculated from equation IV. 1 and the observed periods. At Q the wavelength is 157. 0 meters, and at R it is 75. 3 meters.

For the oscillations under consideration, the maximum particle velocity occurs at the mean depth of the thermocline.

Thus at this depth a maximum electromotive force (emf) is generated due to the water motion through the earth's magnetic field. To first order the particle velocity is zero at the sea surface. The emf established at the mean thermocline depth is then effectively short circuited by the surface water, and an electrical current density is set up in the surface layers. This current density is in phase with the generated emf that is maintained by the oscillating water particles. In the event of motion in the surface layers, other emfs will be induced due to that motion. These voltages will show up as a bias on the oscillating induced emf below, since the surface emfs will either oppose or enhance the current density set up by the dissipation of the oscillatory emf at the mean thermocline depth. The direction of the surface motion relative to the internal wave propagation will directly determine the magnitude of the electrical interaction. If either there is no surface motion or if the surface motion is perpendicular to the direction of wave travel, then the emf set up by the internal oscillations will be totally dissipated in the surface

layers without bias by surface voltages. This total dissipation is assumed to be the case here, although some of the irregularities in the measured electrical signal (Figure 8) are probably due to a certain amount of long period water current bias.

The emf per unit distance generated by the interaction of any velocity field with any magnetic field can be shown to be $(\vec{V} \times \vec{H})$, (by integrating Ohm's law in a nonstationary reference frame around a closed circuit). For observations Q and R, the ship was sailing due east (+x). The component of the emf in this direction can be written (by expanding the cross product),

$$Ex = V_y H_z - H_y V_z$$

$$= H_z(V_y - \Gamma V_z)$$

In the first internal mode, V_y can be neglected relative to V_z. Γ for this area is 2.5, and H_z is 1.2×10^{-5} weber/m^2. Since the surface layers are essentially motionless, this emf can be considered totally dissipated at $Z \approx O$ through ohmic losses. If $\vec{i}$ is the electrical current density and ρ the resistivity of sea water, the x component of surface emf is:

$$(\rho ix)_{z=0} = H_z \Gamma V_z \qquad \text{IV.2}$$

This is the signal measured by electrodes towed at the surface in the x direction.

The amplitude of the measured signal (Figure 8-C) is 2 mv. This corresponds to a maximum vertical particle velocity of 66.7 cm/second. Phillips (1966) shows that, for the lowest internal mode, the amplitude of the velocity potential outside the thermocline is:

$$\phi_{max} = \frac{ia\sigma}{k} \frac{\cosh kz}{\sinh kd}$$

Thus the amplitude, a, of the oscillation can be found in the limit as $Z \rightarrow d$ from the maximum vertical particle velocity. Results of the calculations give for Q an amplitude of 17.0 meters and for R, 17.5 meters.

Although Q and R are similar in period and wavelength, the wave forms themselves are seen to be markedly different. The peaks in R have been attenuated significantly and the troughs seem more acutely peaked. Figure 10 shows the thermocline at Q to be at 25 meters, whereas at R it is only 12 meters deep. Thorpe (1965) (cf. Phillips, 1966, p. 171) has shown that when the thermocline is sufficiently close to the surface ($kd < 1$), the wave crests are flattened and the troughs become sharper. Data gathered by LaFond (1962) in a region of a shallow seasonal thermocline clearly exhibit this effect. The same effect accounts for the difference in wave form between Q and R.

It remains to evince the fact that these oscillations are "lee waves" generated by flow over a ridge. Figure 10-C shows the

Brunt-Väisälä frequency at station 61. It exhibits an even sharper maximum than those at stations 64 and 65 just considered. Other stations in the section exhibit similar characteristics (sharply defined, shallow thermoclines). No periods greater than a few seconds (turbulent noise) were recorded, however, in any other part of this region except at R and Q. This seems to point convincingly to the influence of the bottom in developing these stability oscillations.

C. Conclusions

The results of the analysis at Q and R can be summarized as follows:

	Period (sec)	Wavelength (meters)	Maximum Vertical Particle Velocity (cm/sec)	Amplitude (meters)
Q	160	157	66.7	17
R	165	75.3	66.7	17.5

Although in some cases complicated by other effects, oscillations of a similar character and period to Q and R can be observed in the sample portions of the records shown in Figures 8-A,-B. As the data proceed from higher to lower latitudes, the amplitude of this effect is seen to generally increase. This is consistent with the prediction of equation IV. 2, since Γ increases in magnitude toward the equator. As expected and shown in Figure 11, the thermocline also sharpens with equatorward progress, and this compliments the

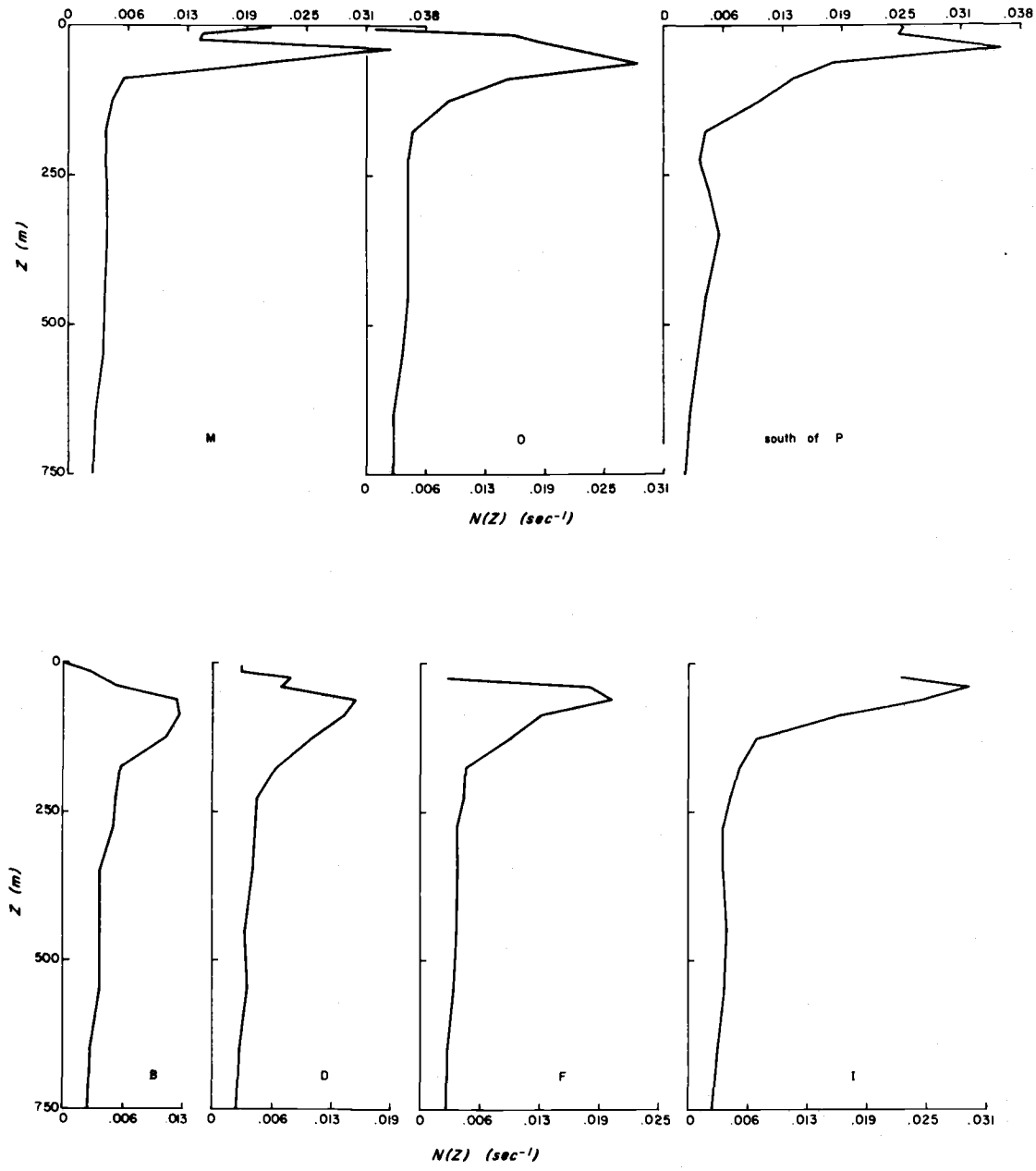

Figure 11. The Brunt-Väisälä frequency as a function of depth for positions indicated in Figure 7.

amplification provided by increasing Γ.

Limited supplementary data prevents a detailed dynamical analysis of these other stability oscillation effects (A through P). However, the important point to realize is that, in the tropics and subtropics, the lowest internal mode oscillations create electrical fields whose effects are significant and observable in the signal measured by towed electrodes.

V. VELOCITY OBSERVATIONS AROUND THE PANAMA BASIN

A. General

The Panama basin is defined bathymetrically by a continuous ridge rising an average 1600 meters in relief and extending from Costa Rica (10°N) to the Galapagos Islands (90°W) and from there to Ecuador. The California Current, Peru Current, Equatorial Countercurrent, and Cromwell undercurrent all flow toward boundaries of this basin. Descriptions of currents in the area have been given by Knauss (1961), Wyrtki (1965), Bennett (1963), Bjerknes (1961), and Wooster and Gilmartin (1961), among others. This chapter describes surprisingly high flows found in this region.

B. Method of Analysis

Once the potential gradient has been measured by towed electrodes, four analytical methods may be considered. The first three are based on comparisons of the measured field with the electric field produced by model water currents. Correlation of model and reality determines the degree of usefulness for these approaches. The fourth method is the inverse technique by which a velocity field is generated analytically to produce the electric field observed. This last procedure is yet to be solved. In examining the first three methods, reference is made to Chapter II, C, where model velocity structures are explicitated. As demonstrated there, the important

factor to consider is,

$$(\rho i)_{z=0} / VH_z \qquad V.1$$

where $(\rho i)_{z=0}$ is the measured surface potential gradient. One way of data analysis is to assume depth penetration of the current, h'/h, which implies a set value of factor V. 1, and allows calculation of current speed, V. This is the classical "k factor" technique. A second procedure is to assume surface current speed, giving a value of factor V. 1, thus defining current penetration, h'/h. Since surface currents are more easily measured than current profiles, the second method seems to yield more utility. The third approach is more general since it allows reasonable analysis when the only data available is the measured potential gradient. Chapter II, D describes this approach.

In January, 1969, the surface electric potential gradient was measured around the Panama basin. Data was analyzed in two ways. Figure 12 shows results obtained by using the "k factor" method, assuming $h'/h \ll 1$ (shallow surface current). Values are plotted at inflection points of the potential function measured. Continuity of the real function assures smooth, bounded variations between points. The method suffers from the assumption $h'/h \lll 1$ which has no solid basis in this case.

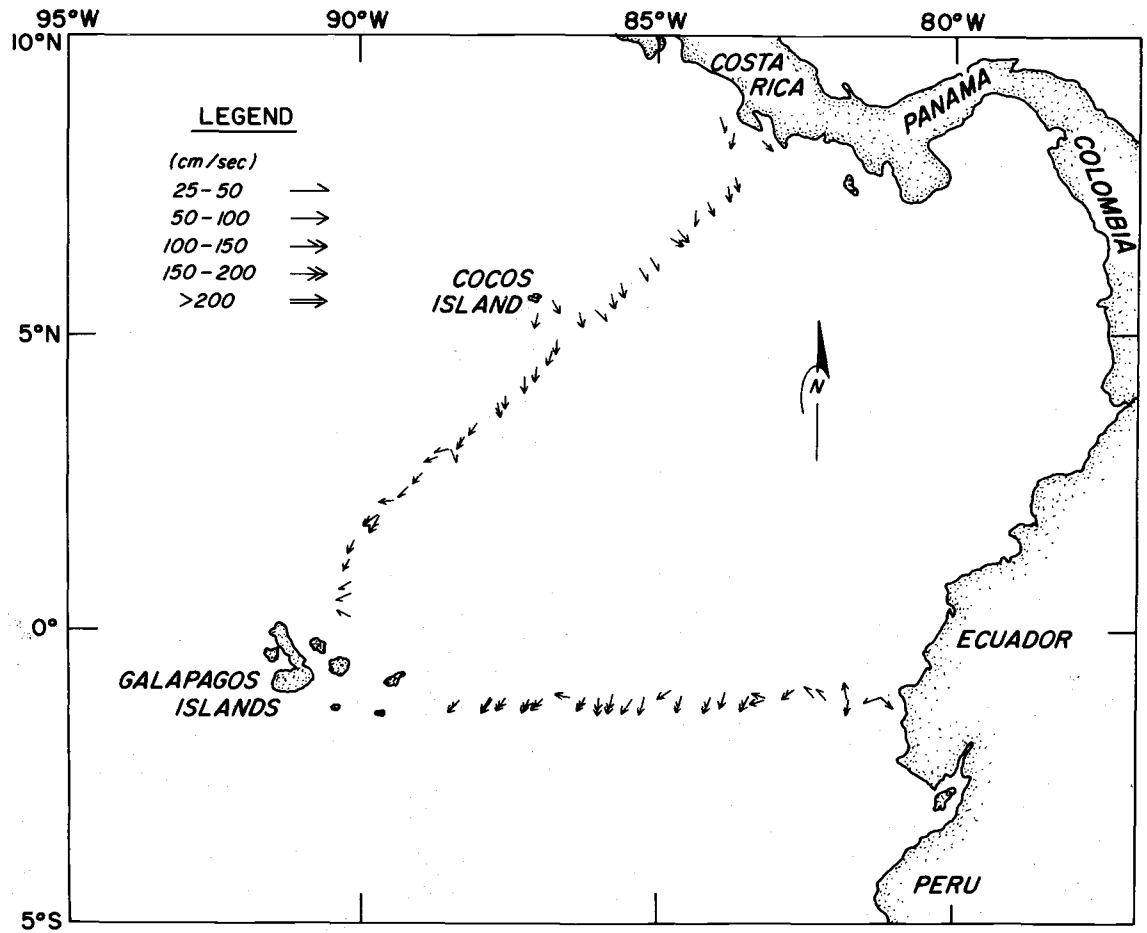

Figure 12. Maximum current vectors measured by GEK along the perimeter of the Panama Basin in the eastern tropical Pacific Ocean.

Figure 13 is a plot of the signal recorded, divided by the vertical magnetic field component along the trackline from Costa Rica to the Galapagos Islands (see Figure 12). Figure 14 is a similar plot for the return eastward trackline to the Ecuadorian coast. The superimposed curves on both figures indicate the smoothed averages of the data shown. The smoothing was obtained by successive arithmetic averaging of the values of each three consecutive data points. This method of averaging is considered adequate for this case since the variation between each data point was linear. For other data and/or applications, other best-fit techniques may be used.

Using the suggested method of analysis given in chapter II, D, the smoothed curves in Figures 13 and 14 have been compared with Figure 1-B which has the correct value of Γ for this geographical location. In this case the comparison was done by directly superimposing the empirical curves over the theoretical ones. Figures 13 and 14 show the results of this comparison, but it is not immediately obvious from the figures, because both curves were coincident within the error shown by the width of the smooth empirical curves in both Figures 13 and 14. The comparison within this error yields a value of $h'/h = 1/4$ for both traverses, and velocities of 72 cm/sec and 136 cm/sec for Figures 13 and 14, respectively. These figures were arrived at by a direct application of the method described in chapter II, D.

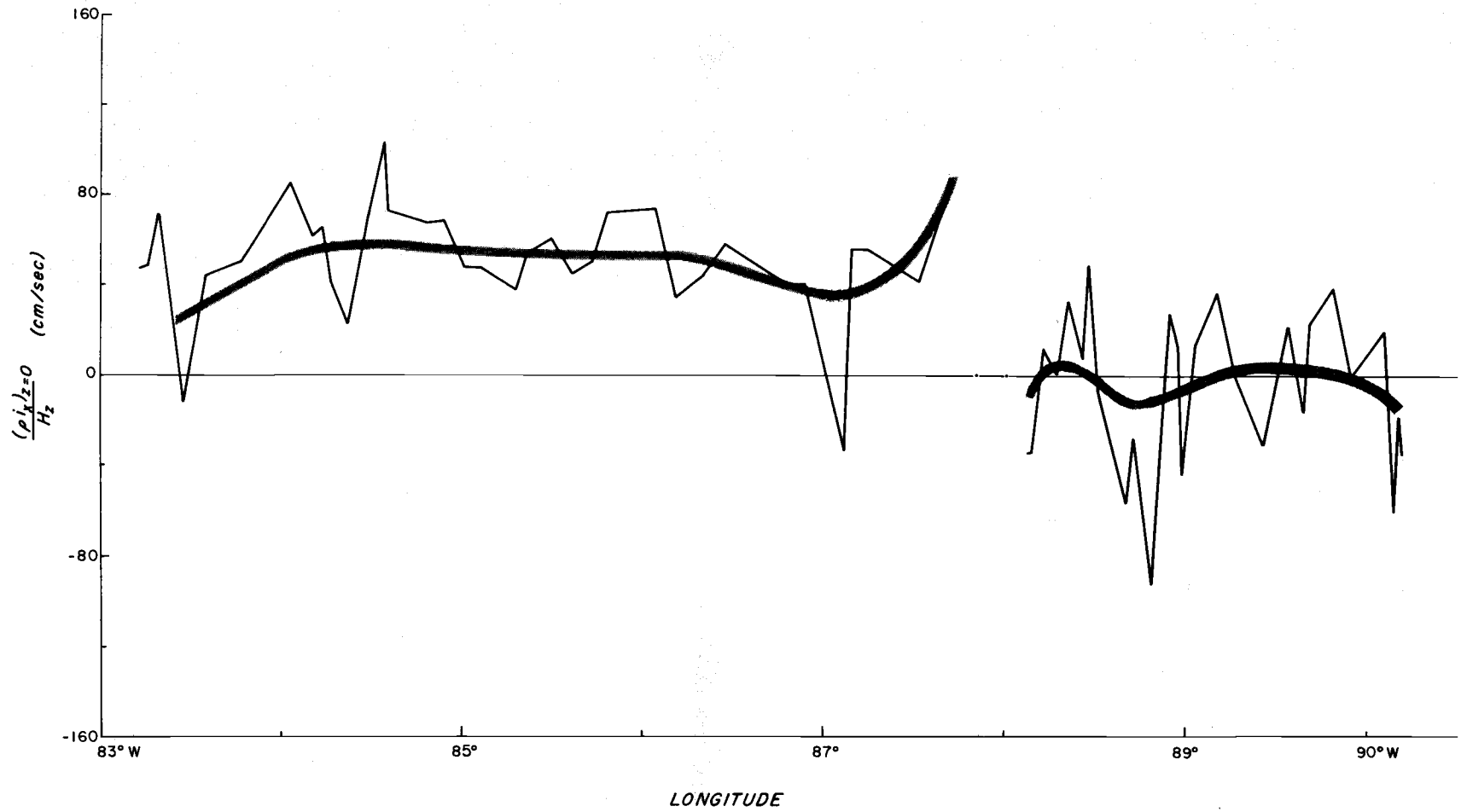

Figure 13. The signal from towed electrodes measured between the Galapagos Islands and the Costa Rica coast. The stippled curve indicates the smoothed average.

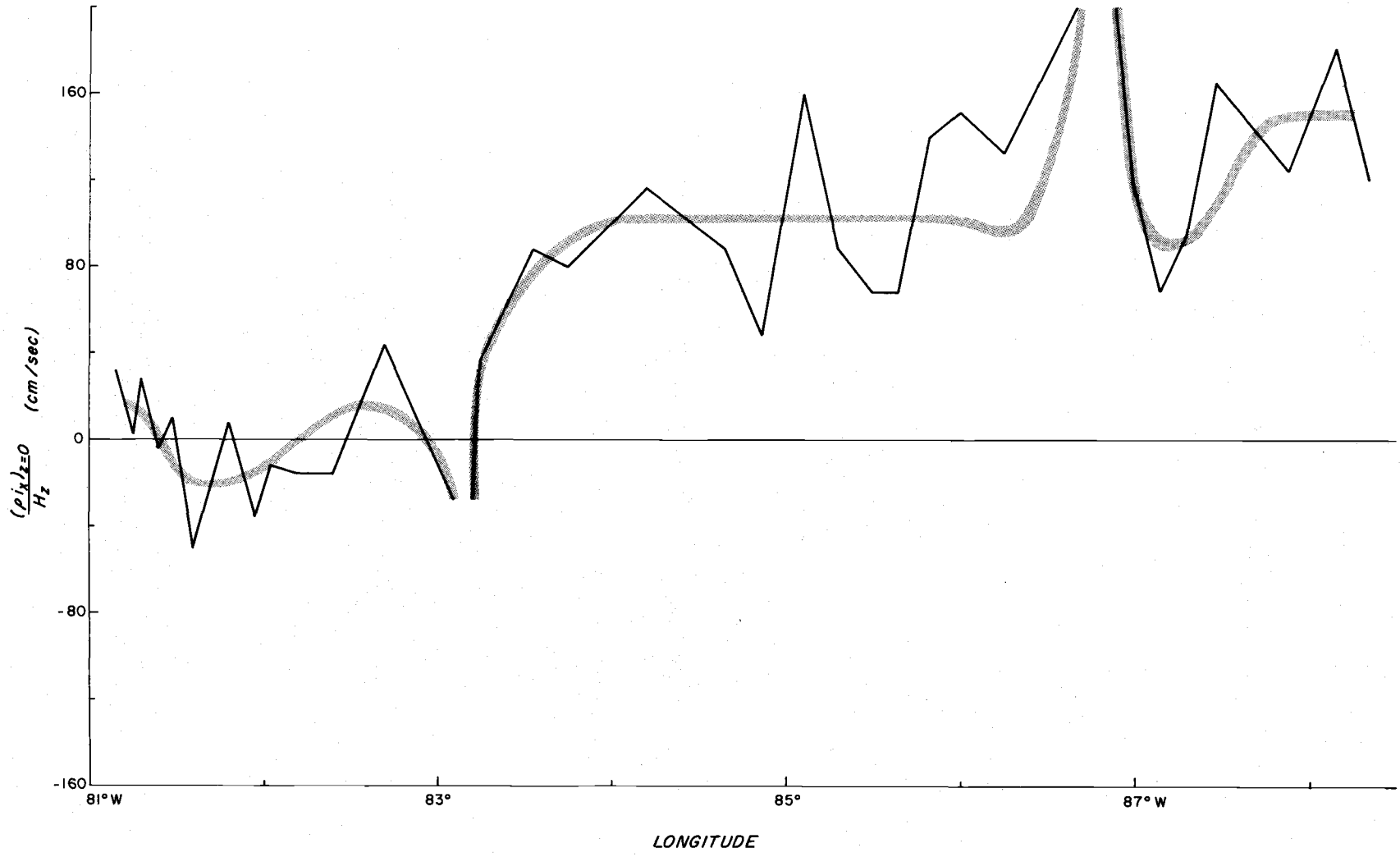

Figure 14. The signal from towed electrodes measured between Ecuador and the Galapagos Islands. The stippled curve indicates the smoothed average.

The conversion of towed electrode signals to velocity values results in a smoothed velocity profile due to the tendency for the recorded signal to be aliased by velocities occurring at all depths in the water column. Thus, except in the case of shallow surface streams, highly accurate values of local velocity are not possible. This limitation is recompensed, however, by the knowledge gained concerning transport. In the present case the velocity structure in the large can be modeled as a rectangular surface stream with a depth equal to 1/4 the total water depth as just shown.

The traverse around this basin is unique from a motional electrical field viewpoint. Since the sail track was directly along the top of a ridge system, the actual water depth directly beneath the ship was considerably reduced. By definition, a ridge is relatively narrow in width, and so immediately adjacent to the ridge (and therefore the path of the ship) the water is much deeper. Electrically speaking, the water immediately adjacent to the ridge provides a readily available, conducting path for any electrical currents developed above the ridge. The depth, h, of previous mention, must always be considered as the total depth of available conducting seawater. For the present data, h is about 2400 meters. The rectangularly averaged current then extends to a depth of 600 meters over the ridge.

From the data shown, transport into the basin from the north

has been calculated to be 188, 000 m^3/sec, and, out of the basin along the zonal trackline, to be 284, 000 m^3/sec. The discrepancy can be accounted for qualitatively. The three "holes" in the system which have not been taken into account in the above transport figures are the two sections immediately adjacent to the coast from shore to about 150 km offshore, and the region surrounding the Galapagos Islands. The currents along the coast seem to be highly variable and their transport is not estimated, although both coastal currents probably have a net transport into the basin (see previous references). Possibly more significant, however, is the Galapagos region. Recent work in this area (Knauss, 1966; White, 1969) indicates the Cromwell current continues east of the Islands in some seasons and may be split into two eastward flowing components. The subsurface nature of this flow combined with a lack of quantitative details of both surface and subsurface flow through the Islands concurrent with the other data make it impossible to even qualitatively estimate the net transport through this third source (or sink). Certainly, the details of the time variable flow are important in developing realistic quantitative models of the circulation in this region.

Figure 15 illustrates a comparison between previously charted currents in this region (Wyrtki, 1965) and those observed by the author. The previous current chart is a compilation of ship drift reports over about a ten-year span. The magnitudes in part B of

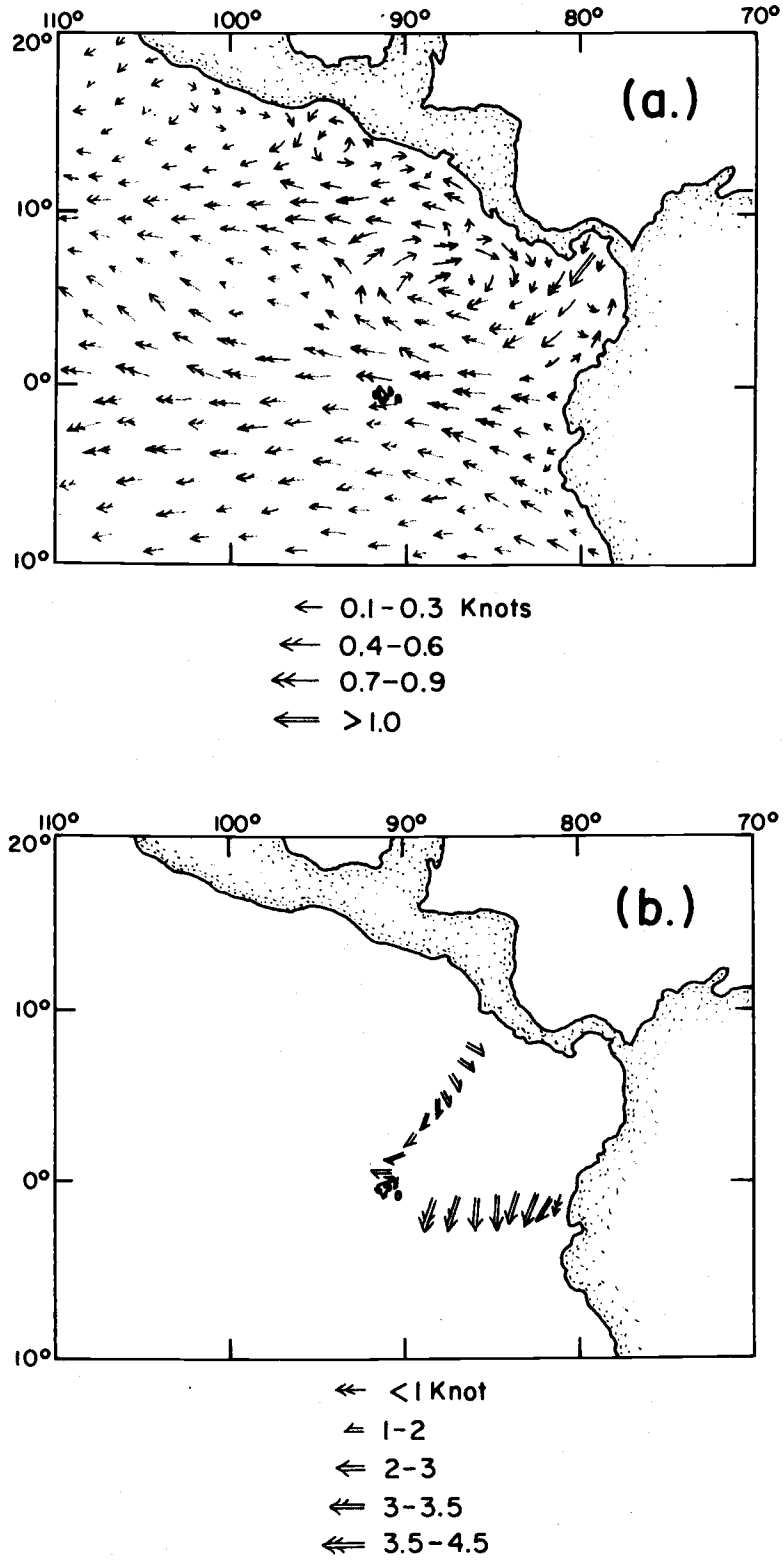

Figure 15. Current pattern for the East Tropical Pacific Ocean. (a) Pattern as previously compiled by Wyrtki (1965). (b) Contrasting strong surface currents recorded by GEK. (Note direction from N and NE)

the figure are averaged from the values shown in Figure 12 and are again maxima. Attention here is called to the direction of the current vectors. As shown in part A of the figure, a large eddy seems to be formed around a point 5°N, 88°W. The recent data (part B) indicate that this eddy has increased in radius and expanded south of the Galapagos Islands. The current directions on the Costa Rica-Galapagos line are evidently consistent with this theory, and their shift in direction parallels that indicated in part A. The Galapagos-Ecuador line shows the velocity with more of a southerly component than would be expected in an imaginary completion of the eddy. This can be accounted for by the expanded flow's interaction with the ridge extending across this line. The ridge decreases the depth by 1000 meters on the average, and conservation of potential vorticity (southern hemisphere) [that is, (local vorticity, ξ , + coriolis force, f,) / (the total depth, D) = constant] shows that the flow immediately on top of the ridge would be turned toward the left. A rough approximation in this case would be that the radius of curvature of the eddy is doubled. The observed data is not inconsistent with this thesis.

These observations indicate that the currents around the periphery of the Panama Basin at this time of year can be described to first order as gradient currents, that is, (in polar coordinates) in the complete equations of motion there are only three relatively significant terms:

$$fV_\theta + \frac{V_\theta^2}{r} = \frac{1}{\rho'} \frac{\partial p}{\partial r}$$

Both the existence of the aforementioned eddy and the proximity of the equator render the centrifugal force term much greater than the coriolis force term (about two orders of magnitude, in this case). Thus, even if the radius of curvature is known, it is impossible to calculate the velocity sections from hydrographic data alone, since the slope of the sea surface remains unknown. To find the slope of the sea surface requires the geostrophic assumption which is in turn a contradiction to the force balance deduced immediately above. The value of the signals produced by towed electrodes is demonstrated for this case, and certainly a more detailed cruise grid using this method is recommended in order to provide a more definitive description of this circulation.

A suggested cruise plan for future current studies in this area using a GEK technique would cover the same basic tracklines shown in Figure 12, but be more complete. Both lines should extend as close to the coast as practical to describe carefully the coastal currents present at the time. A carefully laid out cruise track through the Galapagos Islands in deep water is necessary. Thus, a continuous line from the Costa Rican coast, through the Galapagos Islands and back to the Ecuadorian coast should be run, and then immediately re-run in reverse so high frequency, time-dependent

effects will be averaged. Immediately after this run and re-run, a trackline similar and paralleling this first one except about 25 miles further into the basin should be cruised in the same manner. The results of both these tracks should provide solid information on the water movements in the area at that time. Some further north-south lines would be profitable both to the east and west of the Galapagos Islands to monitor the effect of the Cromwell current. In any current study utilizing the tracklines described above, it is important to obtain measurements as fast and continuously as possible, since time-dependent motion seems to be significant in this area.

VI. SUMMARY AND CONCLUSIONS

Interpreted correctly, measurements from towed electrodes at sea can provide rapid and useful information about an existing velocity field. Under some circumstances this method may be the only practical means to describe the current and transport regime.

It has been concluded from the results of a theoretical review that for deep ocean currents where the conductivity of the bottom can be neglected the best pragmatic interpretive technique consists of modelling the velocity structure two dimensionally either as a rectangular or as a sinusoidally varying function. The towed electrode measured signals produced by such models have been graphically illustrated for both different model dimensions and geographic variables. By a qualified comparison with these theoretical forms, a method of interpreting empirical data is suggested.

Time-dependent magnetohydrodynamical effects have been examined as they pertain to the present study. Hydromagnetic effects have been concluded to be negligible in the ocean. Electromagnetic effects are determined to be unimportant in most cases. Exceptions are motions of large scale (for example, tides), or motions of a more intermediate scale ($\approx$50 km) with shorter periods of variability. The relationships demonstrating the relative importance of electromagnetic effects are graphically shown.

Towed electrode signals are further judged to contain voltage fluctuations due to internal wave motion, especially in lower latitudes. This fact is demonstrated in a kinematic examination of records obtained in the eastern Pacific Ocean between 30°N and the equator. It is shown that the effect becomes more pronounced with decreasing latitude. A dynamic analysis of one observational segment is presented.

Finally, electrical field measurements obtained around the Panama Basin are concluded to be oceanographically unique in a dual sense. Continuous sailing directly along the top of a large ridge system necessitates a wider interpretation of the actual water depth from an electrical viewpoint. Also the existence of an eddy-like velocity structure at this time of year in this region is seen to enhance the value of the towed electrode measurements due to the breakdown of more common techniques, in particular, the dynamic computations.

BIBLIOGRAPHY

Barlow, C. A. and J. R. Macdonald. 1967. Theory of discreteness of charge effects in the electrolyte compact double layer. In: Advances in electrochemistry and electrochemical engineering, ed. by P. Delahay. Vol. 6. New York, Interscience. p. 1-199.

Bennett, E. B. 1963. An oceanographic atlas of the eastern tropical Pacific Ocean, based on data from the EASTROPIC expedition, October-December 1955. La Jolla, California. 165 p. (Inter-American Tropical Tuna Commission. Bulletin. Vol. 8, no. 2)

Bjerknes, J. 1961. "El nino" study based on analysis of ocean surface temperatures, 1935-57. La Jolla, California. p. 219-303. (Inter-American Tropical Tuna Commission. Bulletin. Vol. 5)

Defant, A. 1961. Physical oceanography. New York, Macmillan. 2 vols.

Delahay, P. (ed.) 1961. Advances in electrochemistry and electrochemical engineering. Vol. 1. New York, Interscience. 326 p.

Delahay, P. 1965. Double layer and electrode kinetics. New York, Interscience. 321 p.

Delahay, P. (ed.) 1967. Advances in electrochemistry and electrochemical engineering. Vol. 6. New York, Interscience. 482 p.

Faraday, M. 1832. The Bakerian lecture - experimental researches in electricity. Philosophical Transactions of the Royal Society (London), part 1, p. 163-177.

Hughes, P. 1962. Towed electrodes in shallow water. The Geophysical Journal of the Royal Astronomical Society 7:111-124.

Knauss, J. A. 1961. The structure of the Pacific equatorial countercurrent. Journal of Geophysical Research 66:143-155.

Knauss, J. A. 1966. Further measurements and observations on the Cromwell current. Journal of Marine Research 24:205-239.

Knauss, J. A. and J. L. Reid. 1957. The effects of cable design on the accuracy of the GEK. Transactions of the American Geophysical Union 38:320-325.

LaFond, E. C. 1962. Internal waves. In: The sea, ed. by M. N. Hill. Vol. 1. New York, Interscience. p. 731-751.

Larsen, J. C. 1966. Electric and magnetic fields induced by oceanic tidal motion. Ph. D. thesis. La Jolla, University of California at San Diego. 99 numb. leaves.

Longuet-Higgins, M. S. and N. F. Barber. 1946. The measurement of water velocity by electromagnetic induction. An electrode flowmeter. Teddington, Eng. 22 numb. leaves. (Admiralty Research Laboratory Report ARL/R. 1/102. 22/W)

Longuet-Higgins, M. S., M. E. Stern and H. Stommel. 1954. The electrical field induced by ocean currents and waves, with applications to the method of towed electrodes. Woods Hole, Massachusetts. 37 p. (Woods Hole Oceanographic Institution. Papers in Physical Oceanography and Meteorology. Vol. 8, no. 1)

Malkus, W. V. R. and M. E. Stern. 1952. Determination of ocean transports and velocities by electromagnetic effects. Journal of Marine Research 11:97-105.

Phillips, O. M. 1966. The dynamics of the upper ocean. Cambridge, Cambridge University. 261 p.

Roberts, P. H. 1967. An introduction to magnetohydrodynamics. New York, American Elsevier. 264 p.

Sanford, T. B. 1967. Measurement and interpretation of motional electric fields in the sea. Ph. D. thesis. Cambridge, Massachusetts Institute of Technology. 161 numb. leaves.

Stommel, H. 1948. The theory of the electric field induced in deep ocean currents. Journal of Marine Research 7:386-392.

von Arx, W. S. 1950. An electromagnetic method for measuring the velocities of ocean currents from a ship under way. Woods Hole, Massachusetts. 62 p. (Woods Hole Oceanographic Institution. Papers in Physical Oceanography and Meteorology. Vol. 11, no. 3)

von Arx, W. S. 1962. An introduction to physical oceanography. Reading, Massachusetts, Addison-Wesley. 422 p.

White, W. B. 1969. The equatorial undercurrent, the south equatorial undercurrent, and their extensions in the south Pacific Ocean east of the Galapagos Islands during February-March, 1967. College Station, Texas. 74 numb. leaves. (Texas. Agriculture and Mechanics University. Dept. of Oceanography. Reference 69-4-T. Office of Naval Research Contract Nonr 2119(04))

Wooster, W. S. and M. Gilmartin. 1961. The Peru-Chile undercurrent. Journal of Marine Research 19:97-122.

Wyrtki, K. 1965. Surface currents of the eastern tropical Pacific Ocean. La Jolla, California. p. 271-303. (Inter-American Tropical Tuna Commission. Bulletin. Vol. 9, no. 5)

APPENDICES

APPENDIX A

A NOTE ON ELECTROMAGNETIC UNITS

The scientific method is generally the sum of two equal parts: induction and deduction. There is madness in the order. The deductive process flows only from the apex of the inductive pyramid. Historically, the physics of electricity and magnetism stands as a good example.

Induction is grounded in observation, and thus, inherently depends for its communication on units of measurement. The accumulation of data has usually been characterized by diversity in time and space, multiplicity in applications, and a sometimes frustrating lack of communication. Different and sometimes inconsistent sets of units occasionally result in describing the same physical phenomena.

Electromagnetically speaking, engineers have tended to use a charge-rationalized MKS system of units mainly because it yields quantities compatible to practical measurement instrumentation. With physicists, particularly atomic and nuclear, the gaussian system is frequently used. The gaussian system is, in turn, a hybrid of two earlier systems: the electrostatic system (esu), and the electromagnetic system (emu). Other systems have also been in vogue, at times in the past, but the gaussian and MKS are the most prevalent units used today.

Rationalized MKS units are used throughout this paper. "Rationalized" units are those that include $\eta\pi(\eta = 2, 4, \ldots)$ - type terms within the constants in such a way that π as a factor in problem solutions turns up when it would be expected to due to the geometry of the problem. In non-rationalized units π appears rather unexpectedly and independently of geometrical considerations.

The following table is included as a logical reference in applying and relating the contents of this dissertation with other data. First the fundamental quantities in each system are defined and their inter-relationships demonstrated. A conversion table follows.

TABLE A.1

RATIONALIZED MKS SYSTEM	GAUSSIAN SYSTEM
DEFINITION - Magnetic permeability (in vacuo) = $\mu_o = 4\pi \times 10^{-7}$ weber/amp. m.	
law of Biot and Savart (force between current carrying circuits): $\vec{F} = \frac{\mu_2}{4\pi} I_1 I_2 \phi_1 \phi_2 \frac{d\vec{\ell}_2 \times [d\vec{\ell}_1 \times \vec{r}_{12}]}{\lvert\vec{r}_{12}\rvert^3}$	
DEFINITION - One ampere is the steady current that produces a force equal to 2×10^{-7} newton/meter between two circuits, each carrying the same current and separated by a distance of one meter.	
DEFINITION - One coulomb is the charge transported by a steady current of one ampere flowing for one second.	
Coulomb's Law (Force between charges): $\vec{F} = \frac{1}{4\pi\epsilon_o} \frac{Q_1 Q_2 \vec{r}_{12}}{\lvert\vec{r}_{12}\rvert^3}$	
DEFINITION - Permittivity (of free space) = $\epsilon_o = 8.854 \times 10^{-12} (\text{coul})^2/\text{mt.}\,\text{m}^2$.	
	Coulomb's Law: $\vec{F} = \frac{Q_1 Q_2 \vec{r}_{12}}{\lvert\vec{r}_{12}\rvert^3}$
	DEFINITION - One esu of charge is the charge that experiences a force of 1 dyne when placed one centimeter from an identical charge.
	Law of Biot and Savart: $\vec{F} = I_1 I_2 \phi_1 \phi_2 \frac{d\vec{\ell}_2 \times (d\vec{\ell}_1 \times \vec{r}_{12})}{\lvert\vec{r}_{12}\rvert^3}$
	DEFINITION - One abampere is the current that produces a force equal to 1 dyne/cm. between two circuits, each carrying the same current and separated by a distance of one centimeter.
	$\frac{\text{CHARGE (esu)}}{(\text{TIME})(\text{VOLUME})} \sim i \sim \frac{\text{ABAMPERES (emu)}}{(\text{VOLUME})}$
	CURRENT DENSITY
	$\vec{i}_{esu} = c\vec{i}_{emu}$
	c = speed of light

(TABLE A.1 continued)

RATIONALIZED MKS SYSTEM		GAUSSIAN SYSTEM
CHARGE	1 COUL	3×10^9 esu
CURRENT	1 AMP	3×10^9 esu/sec=10^{-1} abamp.
ELECTRIC FIELD	1 VOLT/M	$1/3 \times 10^{-4}$ dyne/esu
POTENTIAL	1 VOLT	1/300 erg/esu (statvolt)
MAG. INDUCTION	1 WEBER/M^2	10^4 gauss
MAG. INTENSITY	1 AMP-TURNS/M	$4\pi \times 10^{-3}$ oersted (1 gamma = 10^{-5} oersted)
ELECTRIC DISPLACEMENT	1 COUL/M^2	$12\pi \times 10^5$ esu
CAPACITANCE	1 FARAD	9×10^{11} cm
INDUCTANCE	1 HENRY	10^9 emu
MAGNETIC FLUX	1 WEBER	10^8 maxwells

APPENDIX B

SILVER-SILVER CHLORIDE ELECTRODES

STATE-OF-THE-ART

Electrodes used at sea to measure electrical potential have been predominantly of the silver-silver chloride type. In monitoring any potential field using metallic probes, two qualities are highly desirable. First, the inherent potential difference between the two probes when outside the field of interest must be well within the limits of measurement (scale) of the recording instrument. Second, the inherent potential between probes should be stable with respect to both time and environmental changes. Seawater, being a good electrolyte, presents a challenge in satisfying these conditions. So far, this challenge has been most successfully met by silver-silver chloride electrodes.

Manufacture of silver-silver chloride electrodes is relatively simple. Silver oxide is mixed with silver chloride in a 9 to 2 ratio, and the mixture is added to distilled water to form a thick paste. This paste is spread onto some more rigid form, usually made from silver or platinum wire, and fired in a furnace to reduce the silver oxide and form an elemental silver matrix containing silver chloride. Von Arx (1962) describes electrode fabrication using wire gauze as a paste form. Sanford (1967) noted better results using von Arx's

method by increasing the firing temperature from 450°C to 460°C and the firing time from 15 minutes to 20 minutes. Some experiments on geometrical shape of electrodes are reported here.

The problem of maintaining the initial inherent potential difference (between pairs) as small as possible to facilitate measurement is solved by manufacturing many electrodes and choosing the best matched pairs. Considering the present market size and volume turnover of electrodes this method is satisfactory.

By far the most serious problem in using electrodes is their dynamic response to changing environmental conditions. These changes may be divided into two main categories: electrochemical effects due to differences in the state variables of seawater; and hydrodynamic effects due to flow over the electrode surfaces.

Sanford (1967) re-examined the influence of temperature, salinity, oxygen, and pressure on electrode pairs. Several results are of interest. Potential differences arising from temperature and salinity gradients are seen to significantly dominate oxygen and pressure effects. It is shown that, to first order, electrochemical potential differences between silver-silver chloride electrodes (in seawater) are related as

$$\Delta E = \pm 61.18 \frac{T}{S_2} \Delta S \pm (315 + 3.5\Delta T)$$

where ΔE = potential difference in microvolts,

T = temperature in degrees Kelvin,

ΔS = salinity difference = $(S_1 - S_2)$, where $S_2 < S_1$ (‰).

(Second order effects for gradients commonly measurable by towed electrodes are calculated from Sanford's results to be of order $\pm 1\mu V$.)

Using these results with sea-surface parameters typically found across the Gulf Stream, the potential difference between electrodes 100 meters apart due solely to electrochemical effects is calculated for an extreme case. Taking,

$T = 24°C\ (297°K)$
$S = 36.5\ ‰$
$\Delta T = 0.30°C\ (°K)$
$\Delta S = 0.0075\ ‰$
$\Delta E = 320\mu V = 0.32$ mv.

Recent sales literature for commercially available GEK's claim for electrodes a "maximum drift between matched pair, 0.1 mv." Such literature should always be read critically.

In his experiments Sanford used the wire gauze-type electrodes described by von Arx (1962). Equilibration time in response to both temperature and salinity changes is rather large for this design. For thermal emf's, only measurements made 15 minutes or more after any large temperature change were relied on. Figure B-1 shows an example of system adjustment to salinity change. Equilibration time is seen to be in the order of 5 hours.

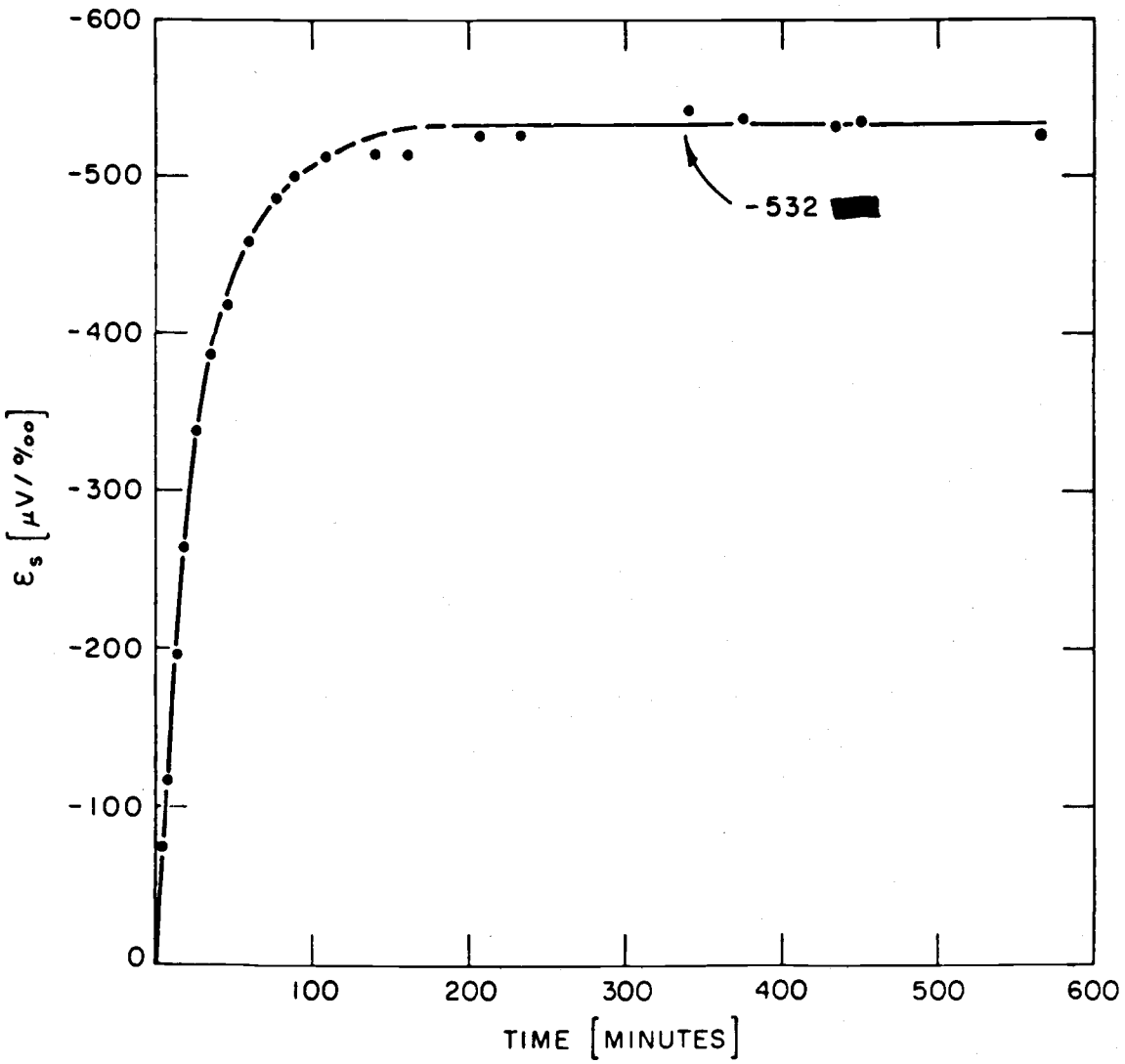

Figure B-1. Potential of sea water concentration cell versus time for S_1 = 37‰ and S_2 = 29.6‰. (After Sanford, 1967)

SOME FURTHER EXPERIMENTS

Silver-silver chloride electrochemical response to major oceanic variables has been relatively well investigated. Potential measurement as a function of electrode geometry or of direct fluid flow near the surface of electrodes has not been described in the literature. Some data has been accumulated in both these areas.

ELECTRODE DESIGN

Several spherical electrodes were fabricated and matched pairs selected to insure minimum initial inherent potential difference. Each electrode consisted of a solid silver ball about 0. 75 cm in diameter into which a silver wire was inserted for connection purposes. The ball was covered with several coatings of silver-silver chloride paste and fired as previously described.

These electrodes were used for several months at sea and their output recorded on a dual channel recorder next to the output from the wire-gauze type of electrode. Results indicated the spherical electrodes unsuitable for use at sea due to their relatively high sensitivity. Their output was much more erratic than the gauze electrodes, and they seemed to be reacting rapidly to small thermal and motional emf's. Several pairs were tried with equivalent results. One possible explanation for the behavior is that this configuration employs a spherical equipotential surface in sensing the electric

field, and small changes in the field affect the entire electrode with very little "electrical inertial lag."

Smaller electrodes were also tried. They consisted of a length of silver wire bent into a small hook at the end. The hooked section was filled with the silver-silver chloride paste and fired as usual.

These electrodes proved to be unsatisfactory due to their inability to come to initial equilibrium when attempting to match pairs of low potential difference. After soaking in seawater for two weeks, pairs were connected to a recording potentiometer for 24 hours. Figure B-2 shows typical portions of the potential difference recorded. Each record obtained contained successive sections similar to those shown in the figure. The order of succession was arbitrary - not from noisy to quiet. The reasons for changes from a relatively stable period to an erratic one were not apparent. As seen in the figure the periods of most oscillations were less than 1 second, and this may have been limited by recorder sensitivity.

The results of these and other electrode construction experiments seemed to verify a statement made by von Arx (1962) that porosity of 60% or more increases stability. This stability is gained, however, at the expense of sensitivity as demonstrated particularly in the large equilibration time illustrated in Figure B-1. It seems as though a better compromise might be able to be achieved by further experiments in electrode design, thus increasing the resolu-

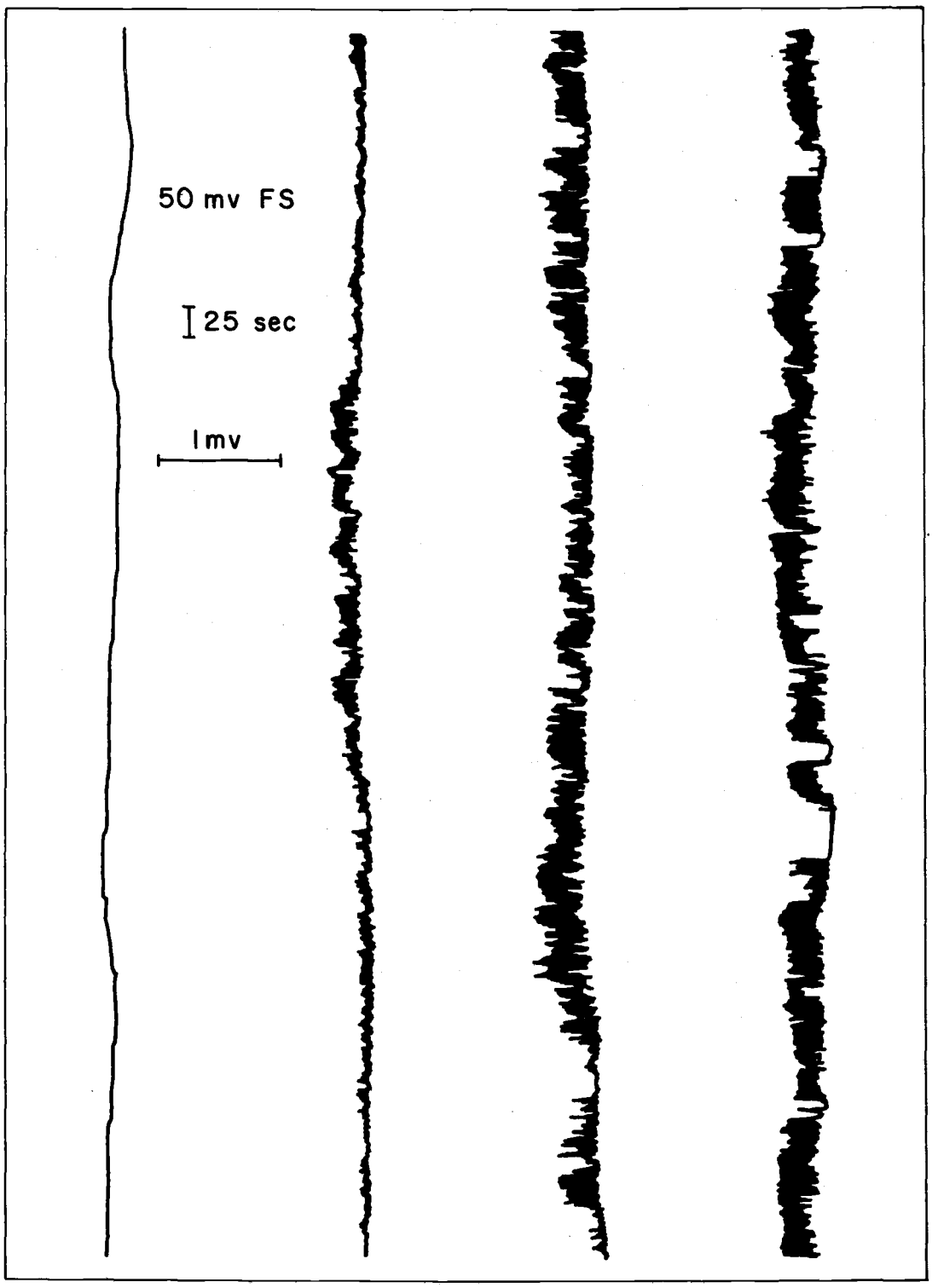

Figure B-2. The potential difference between two well-soaked electrodes (silver-silver chloride) immersed in sea water under completely static conditions was recorded for 48 hours. These are representative portions of the resulting record. Densely inked areas correspond to high frequency pen movement. (See text for details.)

tion of oceanic electrical field measurements without immersing the desired result in the noise. On the whole, research has not been prolific on electrodes for use in seawater to measure potential differences.

ELECTRODE FLOW REACTION

Under normal circumstances electrodes are towed at sea at speeds in the order of 10 to 20 knots. Electrodes are covered with a suitable lagging material (e.g. glass wool) and housed in a protective casing. One example is illustrated by von Arx (1950). The lagging material and encasement have been mentioned (von Arx) as and are usually assumed to be an electrode insulation from response to thermal and saline gradients, that is, a short term protection against non-motional potentials. Another, and more important purpose, however, is protection from direct flow past the electrode surfaces. This has yet to be quantified accurately. Precise determination of this effect would result in an extremely sensitive small-scale flowmeter useful in wave and turbulence measurements. This project is suggested for further research.

Contact potentials of metal electrodes immersed in electrolytes have been well described for specific substances in electrochemistry. Excellent treatments are provided by Delahay (1967, 1966, 1961). Evidently a "double layer" consisting of an outer Helm-

holtz plane and an inner Helmholtz plane forms immediately adjacent to the metal surface and between it and the diffuse bulk electrolyte. The innermost layer is characterized by solvated ions, and the outermost by adsorbed ions. The structures, properties, and dynamics of this double layer is complicated and specifically is a function of the substances involved. Figure B-3 depicts one model of this layer that has been proposed. Although descriptions of the potential distribution caused by this layer are available for certain elements, none have been found for silver-silver chloride electrodes in seawater. Before the emf source due solely to the immersed electrodes can be accurately determined, these properties will have to be described carefully, as a function of both state variables and electrolyte velocity.

Examples of potentials due to flow near electrode surfaces are shown in the accompanying figures. Figure B-4 shows the output of a pair of electrodes placed in a long rectangular wave tank in various orientations. The tank was filled with seawater 3.3 centimeters deep and was about 6 meters long and 0.15 meters wide. The electrodes were suspended from supports across the tank top into the water about 1.5 centimeters from the surface, well away from the sides, and 6 centimeters apart. They were oriented in different directions relative to the water velocity, and the different positions are indicated on the figure (in plan view). Electrodes were connected

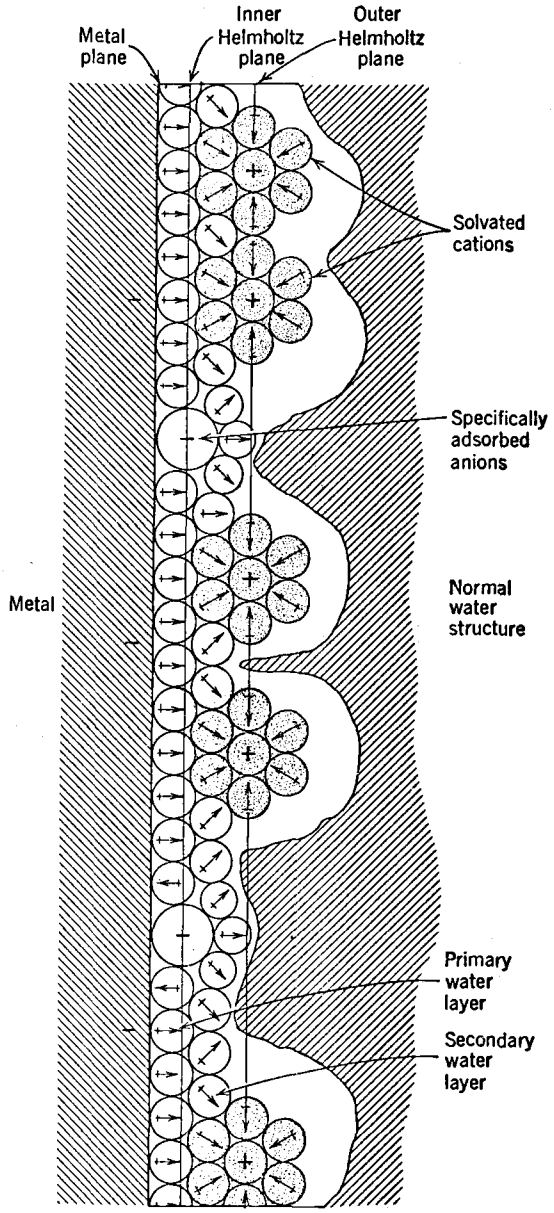

Figure B-3. Hypothetical detailed structure of the electrolyte double layer (Barlow and MacDonald, 1967).

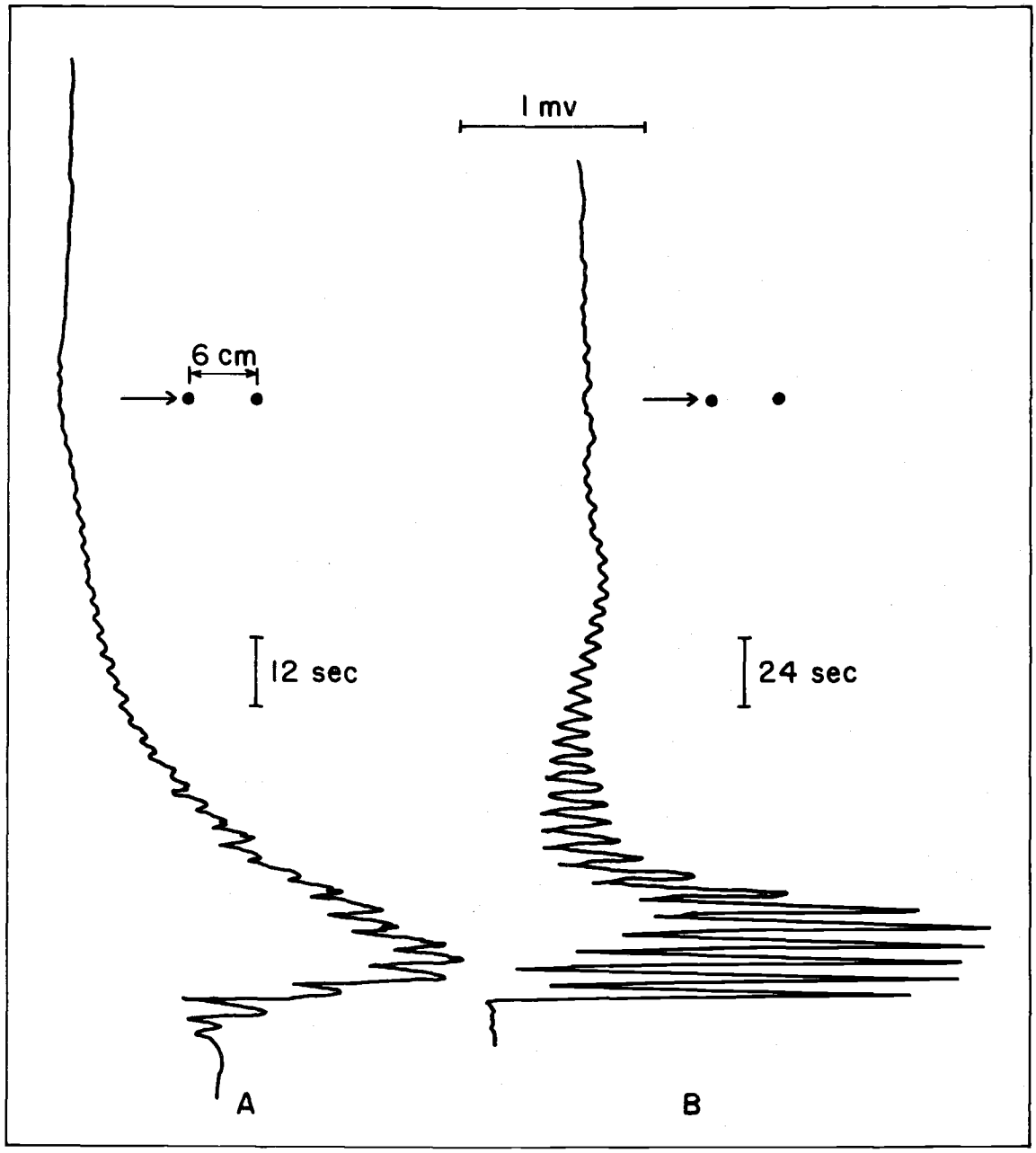

Figure B-4. Electrical potential developed by direct wave-induced flow past silver-silver chloride electrodes in a long narrow tank. Arrows (⟶) indicate direction of water velocity.

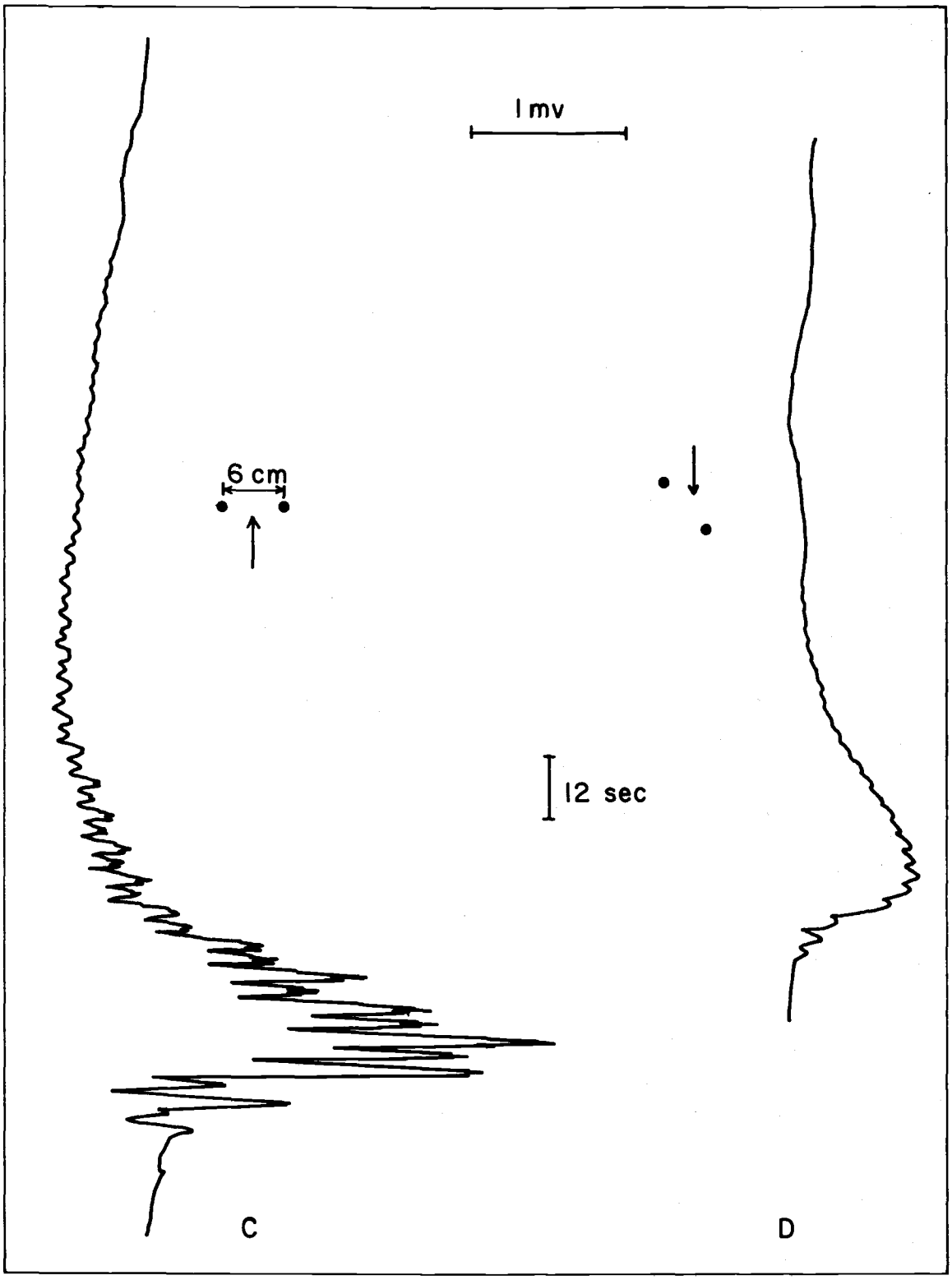

Figure B-4. (continued)

directly to a potentiometric strip chart recorder rated at infinite input impedence. They had been soaking for several weeks in sea-water immediately before the experiment. An impulsively generated wave was introduced into the tank by raising and lowering one end of the tank a short distance in a given time. This produced an initial wave with an amplitude of 1 centimeter that reflected back and forth off the ends of the tank. Of course, after initial reflection, the wave spectrum gained energy at other frequencies and the attenuation was certainly not monochromatic. However, the experiment served to illustrate the point.

All the results show the initial large potential difference generated when the first few and largest waves pass back and forth. The large shift from the static value of potential difference at the first motion and the somewhat exponential return to this static value seems to substantiate the fluid "double layer" idea. Amplitude attenuation of the wave-induced motion is clearly visible, and the differences among electrode orientations is discernable in this re-spect. The physical meaning of these differences was not imme-diately obvious due to the complicated wave spectrum in the tank. A point worth mentioning is the high sensitivity of this system. Motion hardly distinguishable in the tank by eye as the wave almost com-pletely dissipated still produced quite obvious voltage shifts on the recorder.

Under shallow water wave assumptions, the maximum particle velocities in the tank (direction of the arrows on Figure B-3) were calculated to be about 17 cm/sec. Using the results of Longuet-Higgins, Stern, and Stommel (1954), the maximum potential observable due to this wave motion as a source of motional emf in the earth's magnetic field is about 0.1 microvolt. Noting the scale on the figure, it is immediately concluded that the observed changes in potential difference are due to local hydrodynamic effects. This was verified by flow-shielding the electrodes with a porous material (sponge), and repeating the experiment. No shifts of potential difference at all were observed - the recorder pen remaining steady regardless of motions in the tank.

The experiment was also repeated in a larger tank with electrodes spaced 1 meter apart. As it turned out, wave generation could not be adequately controlled and the seawater movement in the tank was complicated and multidirectional (more like the real ocean). Figure B-5 shows an example of a typical observation. More controlled and quantified experiments need to be done.

Maximum water velocity in all of the laboratory work was still relatively slow compared to speeds at which towed electrodes are moved at sea. As just seen, electrical potential magnitudes due to flow effects may be sizable, and precautions must be taken to avoid them. In view of the electrochemical lag times discussed, the main

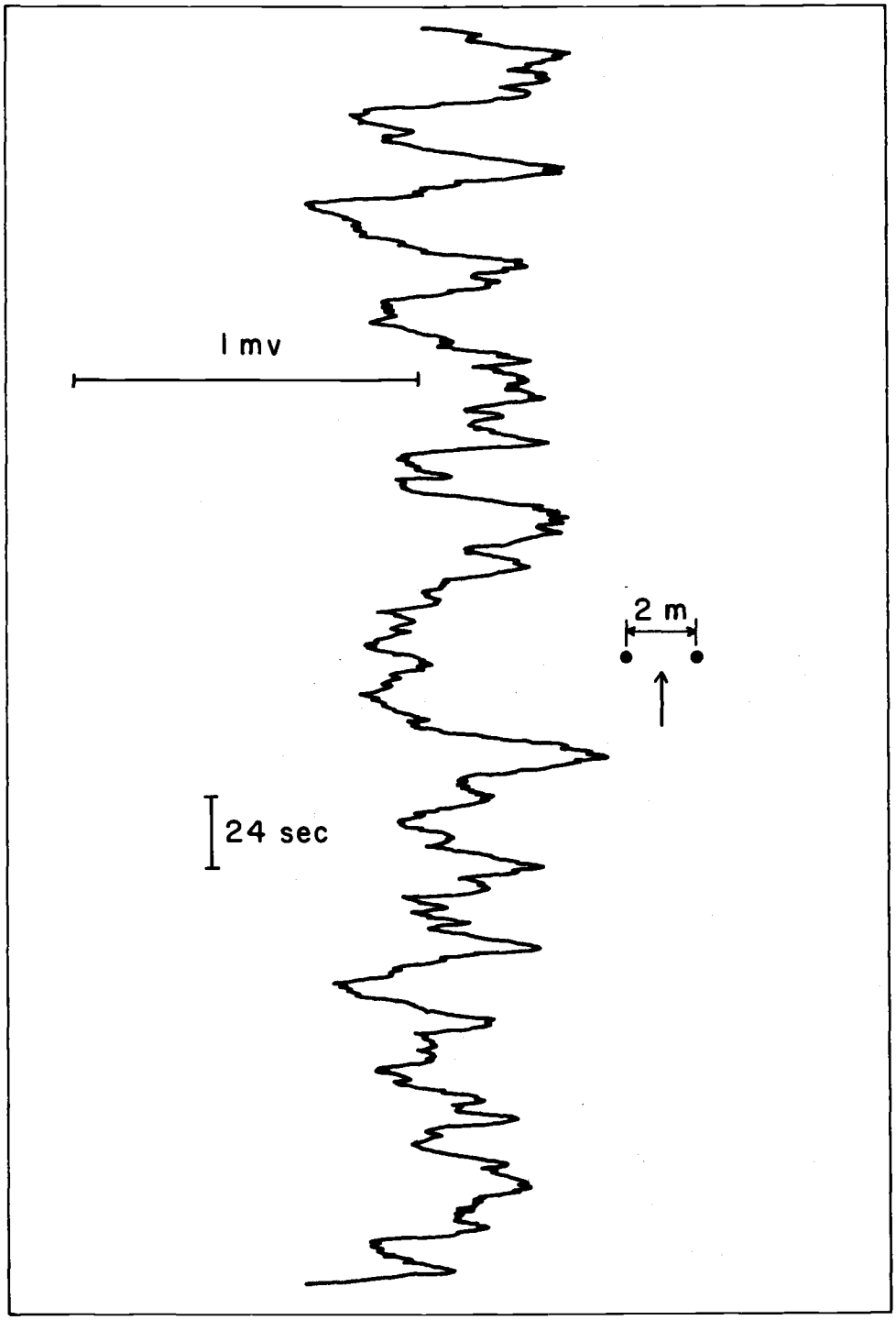

Figure B-5. Electrical potential developed by a complicated flow past silver-silver chloride electrodes in a larger (see text) tank.

purpose of electrode housings and coverings is protection from electro-hydrodynamic effects.